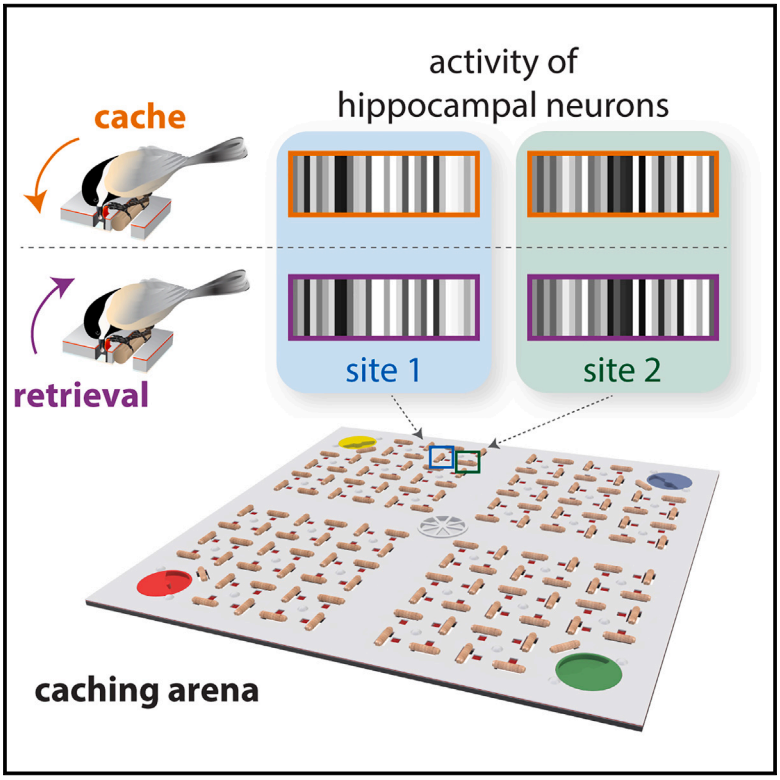
Cell

Article

Barcoding of episodic memories in the hippocampus of a food-caching bird

Graphical abstract



Authors

Selmaan N. Chettih, Emily L. Mackevicius, Stephanie Hale, Dmitriy Aronov

Correspondence

da2006@columbia.edu

In brief

Hippocampal recordings in food-caching chickadees reveal sparse, transient representations of distinct episodic memories.

Highlights

- High-density hippocampal recordings in food-caching chickadees
- Each cache is represented by a unique, sparse pattern of activity ("barcode")
- Barcodes are distinct from and orthogonal to the conventional, smooth place code
- Barcodes reactivate during subsequent retrievals and could encode episodic memories

Chettih et al., 2024, Cell *187*, 1922–1935
April 11, 2024 © 2024 Elsevier Inc.
https://doi.org/10.1016/j.cell.2024.02.032

CellPress

CellPress

Cell

Article

Barcoding of episodic memories in the hippocampus of a food-caching bird

Selmaan N. Chettih,[1,3] Emily L. Mackevicius,[1,2,3] Stephanie Hale,[1] and Dmitriy Aronov[1,4,*]
[1]Zuckerman Mind Brain Behavior Institute, Columbia University, New York, NY 10027, USA
[2]Basis Research Institute, New York, NY 10027, USA
[3]These authors contributed equally
[4]Lead contact
*Correspondence: da2006@columbia.edu
https://doi.org/10.1016/j.cell.2024.02.032

SUMMARY

The hippocampus is critical for episodic memory. Although hippocampal activity represents place and other behaviorally relevant variables, it is unclear how it encodes numerous memories of specific events in life. To study episodic coding, we leveraged the specialized behavior of chickadees—food-caching birds that form memories at well-defined moments in time whenever they cache food for subsequent retrieval. Our recordings during caching revealed very sparse, transient barcode-like patterns of firing across hippocampal neurons. Each "barcode" uniquely represented a caching event and transiently reactivated during the retrieval of that specific cache. Barcodes co-occurred with the conventional activity of place cells but were uncorrelated even for nearby cache locations that had similar place codes. We propose that animals recall episodic memories by reactivating hippocampal barcodes. Similarly to computer hash codes, these patterns assign unique identifiers to different events and could be a mechanism for rapid formation and storage of many non-interfering memories.

INTRODUCTION

The hippocampus is critical for remembering events in a single-shot, "episodic" fashion.[1–3] Episodic memories bind together concepts, actions, and sensory impressions that co-occurred within a single experience. It is not known how the firing of hippocampal neurons implements this function. Theories of episodic memory often depend on place cells,[4] which encode spatial location. Importantly, place cells fire differently even in the same environment, depending on contextual variables like sensory cues,[5–8] task goals,[9–11] and time.[8,12,13] These complex responses are hypothesized to provide a code for episodic memory, in which place cells distinguish between different events, including those occurring in the same location.[7,14]

However, everyday life involves experiencing hundreds of events, often in the same spatial context. To store these memories, place cells would have to rapidly form a new representation every time the animal experienced a memorable event. In effect, the hippocampus would constantly modify its "map" of the same environment. It is unclear whether place cells undergo such incessant remapping in the course of routine memory formation.[15] Activity of place cells does change with experience, but most studies of these changes have focused on slow, gradual learning of an environment[16–21] or on dramatic contextual memories like fear conditioning.[22,23]

An alternative idea is that episodic memories are represented by a mechanism distinct from place cells.[24–28] In this model, place cells provide a relatively stable representation of an animal's spatial and non-spatial context, while additional activity represents specific events within that context. Relatively stable place cells would allow a shared representation of context to associate with many distinct memories.

Testing these ideas has been challenging because it requires a behavior with many memorable episodic experiences. Food-caching birds provide a solution to this problem. These birds specialize in hiding thousands of food items in scattered, concealed locations.[29,30] Retrieval of caches depends on memory, both in the wild[29,31] and in laboratory conditions.[32–34] Memories are accurate with centimeter precision[29,34,35] and can last many days.[36,37] Birds remember not only the location but also the content and the relative time of a cache.[33,38] By convention, these three components ("what, where, when") define a memory as "episodic-like."[39–41] Although cache memories lack some features of human episodic memory, including autobiographical recall,[1] they retain many of the same key features: they form quickly, associate with a specific location, and bind place with other content. Cache memories also depend on the hippocampus,[42,43] which is homologous between birds and mammals[44,45] and enlarged in food-caching species.[46,47]

A major advantage of food-caching behavior is that it contains many discrete, well-defined moments of memory storage that can be examined with neural recordings. Recent studies have found mammalian-like place cells in birds,[48–50] suggesting that hippocampal mechanisms are likely shared across vertebrate

species. However, recordings during food caching have not been previously reported. We set out to record hippocampal activity in a food-caching bird, the black-capped chickadee. We engineered an experimental setup for high-density neuronal recordings in chickadees as they performed large numbers of caches, retrievals, and investigations of cache sites. We examined how the hippocampus represents individual caching events and how this episodic encoding relates to the conventional coding of place.

RESULTS

Neural recordings in food-caching chickadees

Chickadees form new memories during food-caching events. Our first goal was to characterize hippocampal activity during these episodes. We optimized a food-caching setup[34] to obtain exceptionally large numbers of caching events. The setup was an arena with 128 cache sites concealed by cover flaps (Figure 1A). Sunflower seeds were provided to chickadees by motorized feeders that opened for brief periods during a session. Because caching is motivated by the instability of food supply,[51] this schedule encouraged chickadees to cache seeds whenever feeders opened (Video S1). When feeders closed, chickadees spent most of the time hopping around the arena and sometimes "checking" sites by opening cover flaps. Although not explicitly required to do so, chickadees covered most of the arena and used most of the sites for caching (Figure S1). They often retrieved caches, eating some of them and recaching others at different locations. Chickadees also checked sites without retrieving seeds, implying that checks were not simply errors in finding caches.

We recorded behavioral videos from six vantage points using high-resolution cameras. We also developed algorithms for millimeter-precision, 3D postural tracking of points on the bird's body in these videos (Figure 1B; Video S2). A seventh camera was used to detect the contents of the cache sites through a transparent bottom layer of the arena. Automated tracking allowed us to record the chickadee's location, to detect when its beak made contact with a site, and to determine whether seeds were placed or removed at a site.

We defined four types of non-overlapping, stereotyped events (Figures S2A and S2B): caches, retrievals, checks (opening a site cover without caching or retrieving), and visits (landing at a site without opening the cover). Caches, retrievals, and checks usually started right after the bird landed at a site (within 100 ms). To analyze these events, we defined a time window from the opening to the closing of the cover flap. Caches and retrievals were brief (median duration 1.2 s and 1.5 s). Checks were even briefer (typically <200 ms), and we excluded a small fraction of longer checks during which the bird could have interacted with the cached seed. Visit duration was highly variable because birds sometimes remained at a site to rest or eat a seed. We used a 1 s window centered on landing at a site to exclude these longer periods of immobility. Our definitions ensured that all four events were restricted to times when the chickadee was actively moving. In a typical session, chickadees produced many events: 68–149 caches, 66–145 retrievals, 742–1,838 checks, and 434–885 visits (25th–75th percentile, n = 54 sessions, Figure 1C).

Chickadees are small (~10 g) and make dexterous head movements to cache food. To record neural activity, we engineered a lightweight (~1.2 g) miniature microdrive assembly housing a silicon probe. Although the device was chronically implanted, we fully retracted the probe from the brain between recording sessions. This "semi-acute" procedure prevented the typical deterioration of neural signals over time and allowed us to record stable numbers of units, typically for >1 month. We recorded in the anterior hippocampus, which contains abundant place cells in other avian species.[48–50] As in other behavioral tasks and species, hippocampal activity was spatially modulated in our arena during site visits. According to standard definitions, 56% of the neurons were place cells (2,462/4,366 units in 5 chickadees). These cells had similar firing rates, stability, and spatial information to avian place cells in a more conventional random foraging task[48,50] (Figure S3).

Individual neurons respond strongly during caches

Activity during caching events was strikingly different from other time points, with many neurons exhibiting unusually high or low firing rates. We used a Poisson likelihood metric to quantify how strongly each neuron's activity deviated from its mean firing rate. In this measure, increases and decreases in firing rate both produced positive deviations. We then measured the average deviation of firing rates across the recorded population. This measure showed strong peaks around cache times (Figure 1D) and was dramatically higher during caches than during other types of events (Figure 1E). Firing rate deviation was higher even when we compared caches to events selected for roughly similar types of movement by the bird (Figures S2C and S2D).

To understand these large changes in population activity, we separately analyzed putative excitatory and inhibitory cells. These neuronal classes are identifiable in birds using firing rates and spike waveforms.[48] Excitatory cells were largely silent during caches (Figures 2A and 2B). Relative to data in which caches were randomly shifted in time, 64% of cells had a significant decrease in firing rate, and only 6% had an increase (n = 2,528 excitatory units, $p < 0.05$). A typical excitatory neuron fired below its average rate on 93% of the caches, producing zero spikes during most caches.

We analyzed the remaining 7% of the caches, when a neuron fired above its average rate. These "cache responses" scattered throughout the environment and did not obviously relate to the neuron's place tuning (Figure 2A), often occurring well outside of a place field. Cache responses occurred at similar rates in place cells and non-place cells (Figure S4A), suggesting that they engaged not specialized cells but the general hippocampal population. Firing rates during these responses were often exceptionally high. We compared these rates to shuffled data, counting only those shuffles that also had above-average firing rates. Expressed as a percentile of shuffles, cache responses deviated from a uniform distribution with a peak at ~100% (Figure 2C). In other words, excitatory neurons were mostly suppressed during caching but, on a small fraction of caches, fired some of the largest bursts of spikes ever observed in those neurons.

Different excitatory neurons were active on different caches, forming sparse patterns of population activity. Because

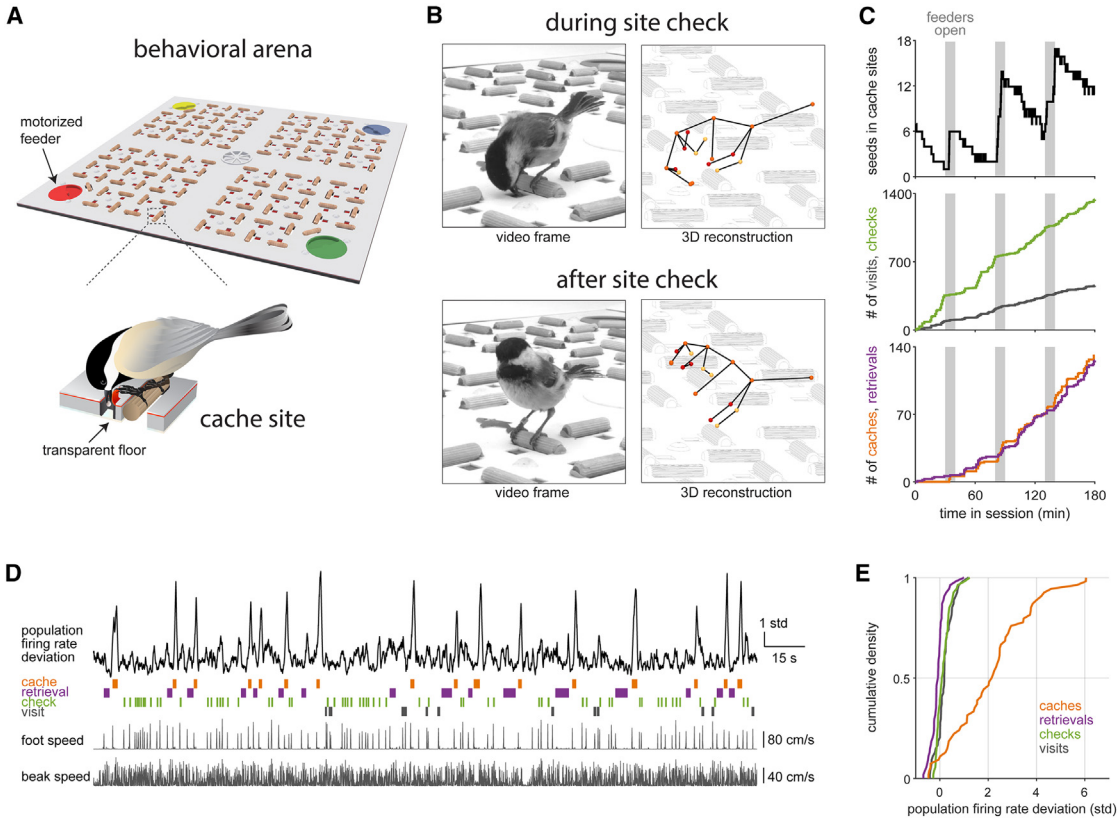


Figure 1. Neural recordings in food-caching chickadees

(A) Schematic of a 76 × 76 cm behavioral arena containing 128 cache sites with 5.3 cm minimum spacing. Each site consists of a perch and a cavity in the floor covered by a rubber flap. The chickadee lifts the cover to interact with a site. Site contents are not visible from above once the cover snaps closed but are camera monitored from below through a transparent floor.

(B) Left: frames from a single video camera. Right: 3D reconstruction using 6 cameras, showing 18 tracked keypoints registered to the model of the arena. Yellow, orange, and red are keypoints on the bird's left, midline, and right. View angle is slightly rotated relative to the video frame.

(C) Behavioral session with three periods during which feeders were open. The chickadee cached new seeds during feeder-open periods. During feeder-closed periods, it retrieved seeds and recached many of them, thus increasing the cumulative number of caches and retrievals throughout the entire session. The chickadee also "visited" sites (perch landing without interacting with the site) and "checked" sites (opening the cover flap without caching or retrieving). Note that seven sites were baited at the start of the session.

(D) Behavior and neural activity during ~4 min of a feeder-closed period. The chickadee frequently hopped between perches (as shown by the peaks in foot speed) and constantly moved its head (as shown by beak speed). Top: quantification of how strongly activity across all neurons deviated from average firing rates. Increases and decreases in firing rate both produced positive peaks in deviation. Firing rates strongly deviated during caches.

(E) Firing rate deviations for the four event types, measured by averaging values in a 1 s window centered at the offset of each event. Medians across events were then computed for each session, and cumulative histograms of the medians were calculated across 54 sessions.

See also Figures S1 and S2.

sparseness could be driven by inhibition,[52] we next analyzed putative inhibitory cells. Just like excitatory cells, inhibitory cells showed highly variable responses across caches, although these responses were not sparse (Figure 2A). Unlike excitatory cells, they could on average be either suppressed or enhanced (33% and 36% of 1,031 inhibitory units, $p < 0.05$; Figure 2D). The strength of this effect was asymmetric: enhanced neurons included extremely active cells that fired above their average rates on nearly every cache (>95%). These cells formed a distinct subpopulation containing 14% of inhibitory units (Figure 2D). Repeating our percentile analysis for inhibitory cells showed that during caching, they produced some of the strongest activity ever observed in these cells (Figure 2E).

Together, our results show that caching engages a distinct state of hippocampal activity. In this state, a subpopulation of inhibitory cells is enhanced, and excitatory cells produce a very sparse pattern of firing across the population. Strong, brief changes to hippocampal firing are often associated with sharp-wave ripples (SWRs).[53] Although mammalian-like SWRs exist in birds,[48] we found that they were exceedingly rare during caches (Figure S5). Caching typically occurred immediately after a bird had arrived at a site, but SWRs happened after prolonged periods of immobility, especially during eating. Caching-related population activity was therefore not obviously equivalent to the network states previously described in the hippocampus.

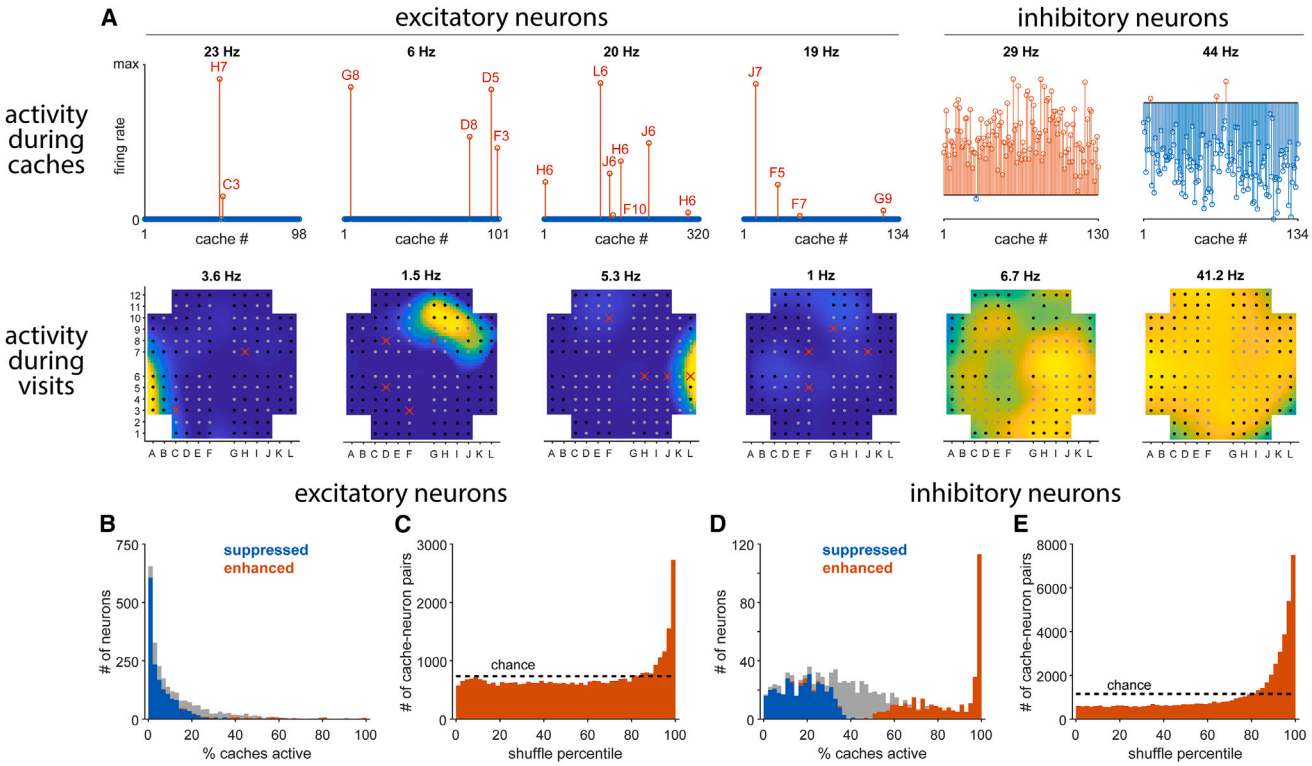


Figure 2. Individual neurons respond strongly during caches

(A) Bottom: spatial maps for six neurons, plotted from zero (blue) to maximum firing rate (yellow). For all cells except the fourth one, maximum is peak rate across the arena; for the fourth ("silent") cell, peak rate is 0.15 Hz but maximum of the plot is 1 Hz. Rate was measured at sites during visits and fit to locations not at sites. Circular symbols, positions of sites; gray circular symbols, sites that were cached into at least once in the session; red "x"s, "cache responses"—i.e., locations where the neuron was active above its mean firing rate. Top: firing rates of the same neurons during all caches. Blue and red stems: caches with firing rates below and above the mean rate. For excitatory cells, cache responses are marked with location to match with the spatial maps below. Cache responses were sparse and not clearly related to place fields. Inhibitory cells were non-sparsely enhanced or suppressed by caching.

(B) Fraction of caches during which an excitatory neuron responded. For most neurons, this fraction was lower than expected from shuffled data. Color indicates neurons that were significantly suppressed or enhanced with $p < 0.05$.

(C) For all cache responses, comparison of firing rate to shuffled data, considering only shuffles with above-average firing rates. Cache responses often exhibited exceptionally high rates.

(D) Same as (B) for inhibitory cells. A subpopulation of inhibitory cells was strongly enhanced by caching.

(E) Same as (C) for inhibitory cells.

See also Figures S3 and S5.

Unique population "barcodes" represent caches

There are two major questions about the cache responses. First, are they consistent for specific locations? In other words, do these responses repeat if a chickadee caches multiple times into the same site? Second, what is the relationship between cache responses and the activity of place cells? To address these questions, we defined a population vector of activity for each caching event. We then measured the correlation of these vectors for pairs of caches at the same site and at different sites. We compared these "cache-cache" correlations to those measured for visits ("visit-visit" correlations).

Visit-visit correlation decayed roughly exponentially with distance between sites (Figure 3A). This is expected from the activity of place cells. Because a typical place field has some spatial extent, correlation of activity is high for nearby sites but lower for distant sites. From here on, we normalized all correlation values by the visit-visit correlation at zero distance—i.e., a normalized correlation of 1 is expected for a pair of visits to the same site. In addition to providing an intuitive measure of correlation, normalized correlation is unaffected by extrinsic factors that vary across experiments, such as the number of recorded units or level of noise.

Cache-cache correlation also decayed at nonzero distances, indicating smooth spatial tuning during caches. Indeed, place cells continued to be active during caching. However, cache-cache correlation sharply deviated from a smooth function at zero distance (Figure 3B). Caches at the same site were correlated with a value of ~4.5. This high correlation shows that responses were consistent across multiple caches into the same site, beyond what is expected from place cells. Signs of this can be seen in individual neurons: for example, the third cell in Figure 2A repeatedly fired during caches into the same sites (H6 and J6).

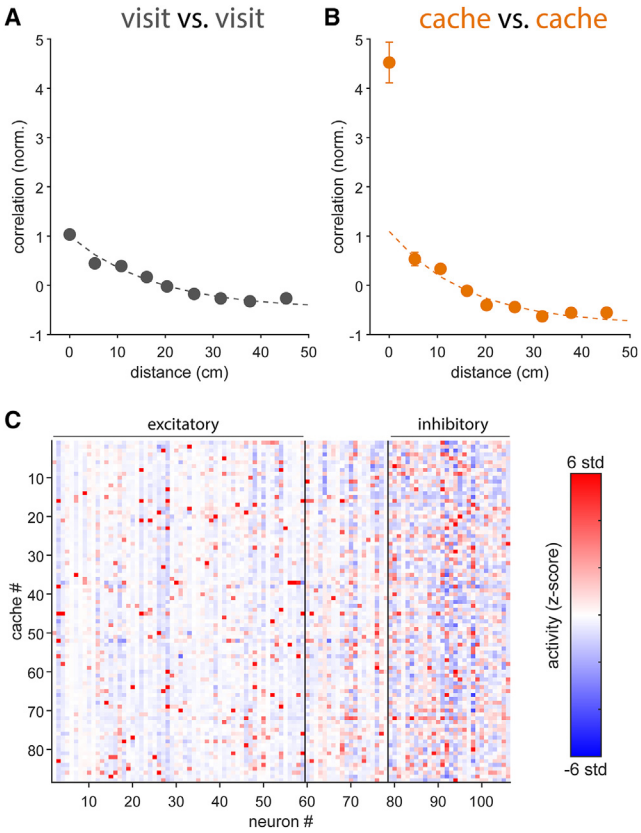


Figure 3. Unique population "barcodes" represent caches

(A) Correlation of population activity for pairs of visits. Correlation decayed gradually, indicating a smooth place code. All correlations are normalized such that the visit-visit value at zero distance is 1 across the dataset. Correlation decayed to a negative value because each neuron's average activity across all visits was subtracted from each population vector. All units, including excitatory and inhibitory, are included in the analysis. Error bars: SEM, not visible when smaller than the symbols. Dotted curve: exponential fit to points at nonzero distances.

(B) Same as (A) for pairs of caches. Correlation showed a strong site-specific component of activity not explained by the place code.

(C) Activity of neurons across caches after subtraction of the place code and the average cache response. We refer to this activity as the "barcode." Firing rates are *Z* scored relative to shuffled data, computed separately for each neuron. Neurons were conservatively classified as excitatory or inhibitory, with some neurons left unclassified.

See also Figure S4.

Notably, correlation was elevated for caches only at the same site. Correlation even between adjacent cache sites (just ~5 cm apart) was much lower and consistent with the value expected from place cells, whose activity was partially correlated at 5 cm distances (i.e., compare Figures 3A and 3B). The sharp peak in correlation implies that cache responses of individual neurons were spatially isolated and did not significantly cluster (Figure 2A). These spatially punctuated responses were markedly different from place fields, which typically extended over multiple nearby sites. We confirmed this increase in spatial specificity during caching using population decoding (Figure S4E).

Our observations suggest two patterns of population activity in the hippocampus. One pattern is the conventional, spatially smooth "place code." The place code is similar for nearby sites and is engaged during both visits and caches. The second pattern is highly specific to an individual site and uncorrelated even between adjacent sites. It occurs only when the bird is caching a seed but not when it simply visits the same site. We call this site-specific, transient activity a "barcode." A barcode uniquely represents a cache site and involves increased firing in a sparse subset of neurons against a background of suppression in the remaining neurons. Notably, the place code and the barcodes engage the same population of neurons in the hippocampus (Figures S4A–S4D).

Because cache responses combined place code and barcode activity, we developed a procedure for separating these two components. To estimate the place code at a site, we temporarily left that site out and spatially interpolated activity at other sites. Repeating this procedure for all sites produced a spatially smooth function over the environment—i.e., the place code. To estimate the barcode, we subtracted the place code from activity recorded during caches. Figure 3C shows a matrix of residuals after subtracting the place code and the average across caches. Excitatory cells in this matrix are mostly silent but occasionally show strong responses. Therefore, their activity appears as sparse positive values (red) on top of negative vertical bands (ranging from white to blue). Inhibitory cells show a mix of positive and negative responses. The population vector, represented by each row of the matrix, is what we call the barcode.

Barcodes reactivate during site interactions

What is the purpose of barcodes? Our hypothesis is that a barcode represents a memory formed by caching at a particular site. In this case, one might expect barcodes to reactivate during other behaviorally relevant times. A reasonable starting point is to compare caches with other events at the same site. We therefore considered retrievals, checks, and visits.

Activity was strongly correlated between caches and retrievals at the same site (Figure 4A). This correlation began increasing ~250 ms before the bird's beak touched the site and continued for the duration of the two events. There was a similar, but briefer, reactivation between caches and checks (Figure 4B), reflecting the shorter duration of the checks. In contrast to retrievals and checks, visits were much more weakly correlated with caches (Figure 4C). This weak but positive correlation of ~1 is expected from place coding during both caches and visits. These analyses show that cache-related activity indeed reactivated, specifically during retrievals and checks—i.e., those events when the bird accessed the contents of the site. Reactivation was transient and precisely aligned to behavior.

We also found that reactivation was highly site specific. There was no strong correlation between caches at one site and events at adjacent sites (~5 cm away; Figures 4D–4F). For all events, correlation with caches decayed exponentially as a function of distance (Figures 4G–4I). For retrievals and checks, however, correlation deviated above the smooth exponential at zero distance. This suggests that the smooth place code was active

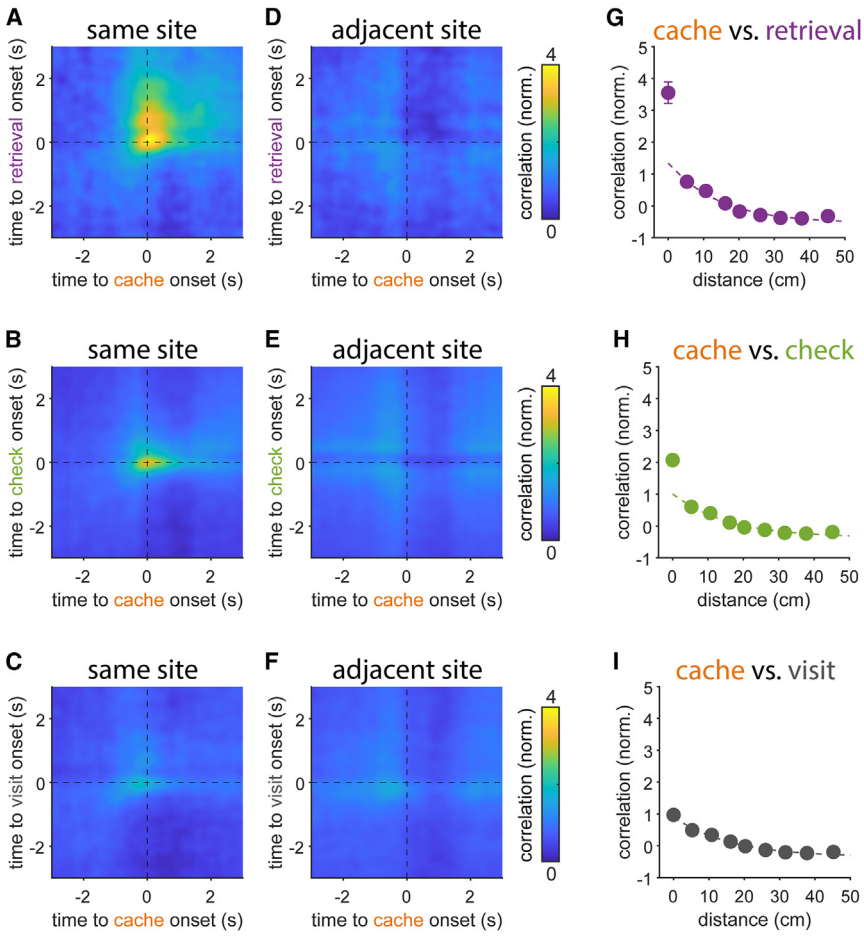


Figure 4. Barcodes reactivate during site interactions

(A) Correlation of activity during caches with activity during retrievals at the same site, averaged across all cache-retrieval pairs. Zero is the time that the bird's beak made contact with the site cover. Population activity vectors were smoothed with a Gaussian window (σ = 100 ms). Activity transiently reactivated between the two events. The shape of the reactivation peak was asymmetric because retrievals were on average longer and had a heavy-tailed distribution of durations.

(B) Same as (A) but for cache vs. check comparison.

(C) Same as (A) but for cache vs. visit comparison. Correlation was weaker and consistent with reactivation of the place code.

(D–F) Same as (A)–(C) but comparing caches with events at adjacent sites (~5 cm away). Reactivation was weak in all cases.

(G–I) Correlation of activity during caches with activity during other events as a function of distance between sites. There was a gradual decay in all cases, demonstrating the presence of a smooth place code. During retrievals and checks, there was also a reactivation of the site-specific barcode. Error bars: SEM, not visible when smaller than the symbols.

during all events, but there was an additional reactivation of the barcode during retrievals and checks. We confirmed this by isolating the barcodes from the cache responses using the procedure described above and by correlating neural activity to these barcodes. Correlation to the barcodes was high for retrievals and checks at the same site (3.0 ± 0.25 and 1.6 ± 0.14, mean ± SEM, n = 54 sessions) but lower for visits (0.55 ± 0.10), including visits that were matched to retrievals in duration or other features (Figure S4F). Correlation of the barcode to events at adjacent sites was low (0.25 ± 0.06, 0.17 ± 0.02, and 0.07 ± 0.02).

We also adapted this analysis to determine how strongly individual neurons contributed to barcode reactivation. Responses formed a continuum across the population, with no evidence of clustering that could warrant dividing cells into "barcode" and "non-barcode" neurons. This is similar to "place cells," which are defined as neurons above an arbitrary statistical threshold on a continuum of spatial selectivity. Using a similar statistical threshold, we found that 29% of excitatory and 30% of inhibitory neurons contributed strongly to barcode reactivation. Place coding and barcoding fully mixed in the population, with no relationship between a neuron's strength of participation in the place code and the barcode (Figures S4B–S4D).

Barcodes represent specific caching episodes

Why do barcodes reactivate? An intriguing possibility is that a barcode represents a cache memory, which is recalled at behaviorally relevant times like retrievals and checks. However, an important consideration is that caches, retrievals, and checks are similar; for example, they involve similar motor actions by the bird. Therefore, an alternative possibility is that the barcode is not related to memory but represents the conjunction of a particular action with location. One way to distinguish these possibilities is to compare different caching events that occurred at the same site. If barcodes represent specific events, they should be different even between caches at the same site. If barcodes represent the conjunction of action with location, they should be identical across these caching events.

We found systematic differences between barcodes at the same site. Barcode-barcode correlation was high for pairs of consecutive caches but decreased for pairs separated by intervening caches (Figure 5A). This effect could result from the animal's experiences (i.e., intervening caches) or from a drift in neural activity over time. To distinguish these possibilities, we analyzed consecutive barcode pairs as a function of the time interval between them (Figure 5B). This analysis revealed two phenomena. First, correlations were elevated for pairs separated by less than 5 min. This effect was independent of location and not specific to caching—i.e., hippocampal activity was generally correlated on an ~5 min timescale (Figure S6A). Second, correlation remained high at long intervals, asymptoting at ~5. This value exceeded the correlation between barcodes separated

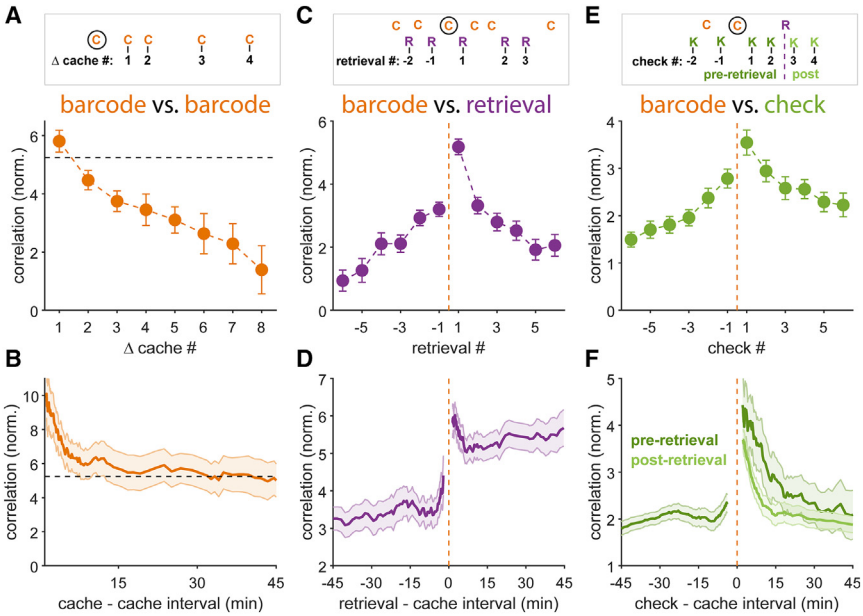


Figure 5. Barcodes represent specific caching episodes

(A) Top: schematic of the analysis. Analysis compares barcodes during caches ("C") that occurred at the same site but at different times. "Δ cache #" is the separation of a cache from the one indicated by the black circle: e.g., 1 indicates two consecutive caches, 2 indicates two caches separated by one intervening cache, etc. Bottom: average correlation of barcodes as a function of Δ cache #. Increasingly separated caches had increasingly different barcodes.

(B) Correlation of two consecutive caches as a function of their separation in time. The trace asymptoted at a high value (horizontal dotted line, also replicated in A), indicating that barcodes became less similar not due to elapsed time but due to intervening caches.

(C) Top: schematic of the analysis, with retrievals ("R") assigned a retrieval #. Retrieval #1 is "matched" to the cache indicated by the black circle. Bottom: correlation of the barcode to the retrieval as a function of retrieval #. Matched retrieval (#1) had the strongest correlation to the barcode.

(D) Correlation of the barcode to retrievals immediately preceding and following a cache (#s −1 and 1) as a function of their separation in time from the cache. The barcode most strongly correlated to the subsequent retrieval, and this effect was stable for long time intervals.

(E) Same as (C) but for checks ("K"). The barcode most strongly correlated to the check that immediately followed the cache.

(F) Same as (D) but for checks. Checks are analyzed separately depending on whether they occurred before or after the retrieval that followed the cache. Barcode reactivation during checks was strong immediately after a cache but did not persist at long time intervals. The decay in reactivation strength was even faster after the seed was retrieved.

Error bars in all panels: SEM.

See also Figure S6.

by intervening caches (compare values in Figures 5A and 5B). In other words, even if two consecutive caches were far apart in time, their barcodes were more similar than if there was an intervening cache. Therefore, barcode-barcode correlation decreased due to the animal's experience rather than elapsed time. We confirmed these results using a linear mixed-effects model (Figure S6B). In summary, barcodes were distinct across caching events at the same site.

This analysis suggests that a barcode does not simply represent caching at a particular site but encodes a unique caching event—i.e., an episode that existed only once in the chickadee's life. To further test this idea, we asked whether barcode reactivations were also distinct across retrievals at the same site. At each site, a chickadee produced some sequence of caches and retrievals. In this sequence, a "matched pair" was a cache paired with the first retrieval that followed it. We reasoned that the recall of a cache memory should most likely occur during its matched retrieval. We found that barcode-retrieval correlation was indeed strongest for matched pairs (Figure 5C). Correlation was weaker for all later retrievals as well as for retrievals that preceded the cache. In other words, activity during a retrieval reactivated the barcode of a highly specific, correctly matched caching event.

Can this effect be explained by temporal proximity of the cache and its matched retrieval? Across our dataset, matched pairs of caches and retrievals were separated by a wide range of time lags, from seconds to tens of minutes. We therefore analyzed correlation as a function of this time lag (Figures 5D and S6C). Again, there was a short-latency effect in the data: caches and retrievals were more correlated when separated by less than ~5 min. However, reactivation remained stronger for matched pairs, even at lags of 45 min.

In summary, the hippocampus produced a distinct barcode during each caching event. This barcode reactivated during a subsequent retrieval from the same site. Reactivation occurred even after long delays. These results suggest that the barcode represents a specific episodic experience, unique in place and time in the chickadee's life.

We repeated these analyses for checks. Barcode-check correlation was also stronger for checks that followed the cache (Figure 5E). However, reactivation during checks was not as persistent as during retrievals. Barcode-check correlation decayed to baseline with a timescale of 13.8 min (Figure 5F, dark green trace; Figure S6D). Note that this does not imply that memory disappeared; in fact, a retrieval after this time would reactivate the barcode. Rather, reactivation was context dependent: sometime after caching, reactivation stopped occurring during checks and only occurred during retrievals. After retrieval, the barcode-check correlation decayed even faster, with a timescale of 5.0 min (Figure 5F, light green trace; Figure S6E). In other words, once a cache was retrieved, the hippocampus quickly stopped reactivating the corresponding barcode.

Place code is unaffected by caching

Our results show that cache memories are represented by barcodes. Are caches additionally represented by the place code?

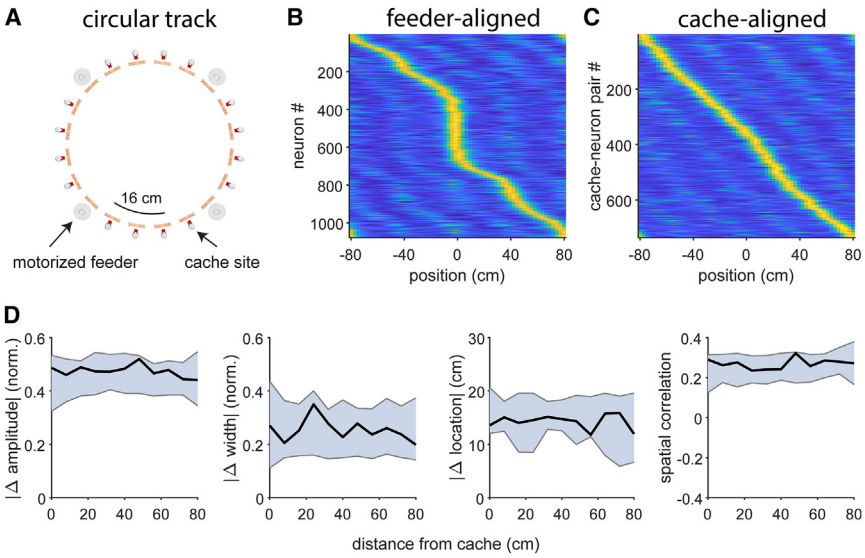


Figure 6. Place code is unaffected by caching

(A) Schematic of the arena for analyzing the effect of caching on place cells. The arena is similar to the one shown in Figure 1 but has cache sites arranged along a circular track of 160 cm circumference with 8 cm spacing.

(B) Alignment of activity to the rewarded feeder, which was changed on a session-by-session basis. Each row is a neuron's spatial tuning curve around the circular track, unwrapped. Rate is normalized from 0 (blue) to the peak (yellow) for each cell. For clarity, only neurons that had a peak firing rate exceeding 3 standard deviations of the entire spatial tuning curve are shown. Place fields were overabundant near the rewarded feeder. Note that due to arena geometry, activity has some 4-fold symmetry: outside of their main place field, some cells produce smaller firing fields in the same location relative to the other three feeders.

(C) Alignment of activity to sites containing cached seeds. Place fields were not overabundant near caches.

(D) Effect of caching on spatial firing. For each neuron, we compared spatial tuning curves before and after a cache using four metrics that were sensitive to the amplitude, width, location, and shape of the firing fields. Black traces: averages across all neuron-cache pairs as a function of the distance between the neuron's peak firing rate from the cache. Shaded areas: 99% confidence interval computed by shuffling cache times. All measures were within the shuffle distribution, demonstrating that caches did not produce significant changes to place tuning.

Place maps change in experience-dependent ways across a number of experimental conditions.[16–21] We thus asked whether place-cell firing was different before and after caching. This analysis was challenging in our 2D arena because obtaining 2D maps requires sufficient coverage of the environment both before and after a cache. We therefore designed a 1D version of the arena in which chickadees moved and cached around a circular track (Figure 6A). The advantage of this track was repeatable behavior: birds typically visited the same site many times before and after each cache, allowing a comparison of activity across many trials. We recorded in 7 additional chickadees, using calcium imaging with a head-mounted microscope.

In rodents, place fields shift with experience and become overabundant near rewards.[17,20,54] We first asked whether chickadee place fields similarly clustered around food sources and/or cache locations. The food source in our experiment was one of four feeders selected on a session-by-session basis. We first rotated each neuron's spatial map around the circular track such that the map was in feeder-centered coordinates with the rewarded feeder at 0°. Consistent with rodent data, place fields in these coordinates were non-uniformly distributed ($p < 0.001$ Kolmogorov-Smirnov test, Figure 6B), with overabundance around the rewarded feeder. We next considered caches and analyzed activity during the time period when a site contained at least one seed. For each cache, we rotated spatial maps such that they were in cache-centered coordinates with the cache site at 0°. Place fields in cache-centered coordinates did not deviate from a uniform distribution ($p = 0.12$, Figure 6C) and were more uniform than in feeder-centered coordinates ($p < 0.001$). Thus, although the place map reorganized around food sources, it was not influenced by caches.

We also looked for other types of changes to the place map in response to caching. Across published experiments, place fields have been observed fully remapping,[6,7,22] changing their firing rates,[7,9,10] changing their widths,[55,56] changing their shapes,[55,57] or shifting their locations.[17,20,54] Caching did not trigger any of these changes (Figure 6D). Spatial patterns before and after a cache were not more different than expected from randomly shuffling cache times. Although we cannot rule out more subtle effects, cache memory seems to be mainly represented in the transient barcode rather than in the place code.

Hippocampal neurons respond to cached seeds

So far, we have focused on activity patterns that are spatially selective. These patterns include place codes and barcodes. However, neurons also had non-spatial changes in activity. Earlier, we showed that many cells were suppressed or enhanced on average across all caches, regardless of the site location (Figure 2). What causes changes to the average firing rate during caching? We examined whether these changes might encode a non-spatial aspect of the chickadee's experience.

An important variable for the chickadee is the presence or absence of a seed in a site. Checks provide an opportunity to study this variable because chickadees check occupied sites that contain a cache as well as empty sites. We found that many neurons fired at different rates during occupied and empty checks, regardless of site location (Figure 7A). These differences were especially prominent in inhibitory cells: they were significant in 36% of the inhibitory and only 4% of the excitatory units ($p < 0.01$). We defined the "seed vector" as the difference in population activity between occupied and empty checks. We then measured the strength of the "seed response" by projecting population activity onto this vector (i.e., computing the dot product with the seed vector). This response was cross validated by

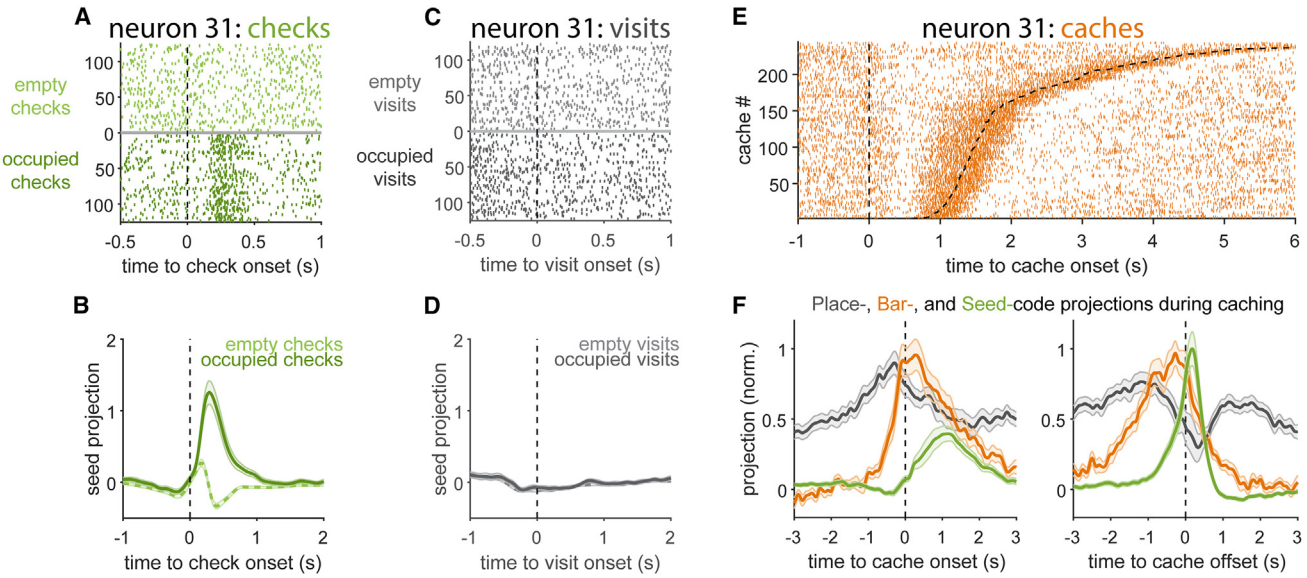


Figure 7. Hippocampal neurons respond to cached seeds

(A) Raster plot of activity during checks. Zero is the time that the bird's beak made contact with the site cover. For display purposes, the same number of empty and occupied checks was selected randomly from the session. The neuron showed a response to the seed in the site.

(B) Average projection of neural activity onto the "seed vector," defined as the difference in population activity between occupied and empty checks.

(C) Activity of the same neuron as in (A) but during visits. Response to the cached seed is absent.

(D) Same as (B) but for visits.

(E) Activity of the same neuron as in (A) and (C) but during caches. Caches are ordered by duration, with both onset and offset shown (dashed lines). The neuron responded around cache offset.

(F) Average projection of neural activity during caches onto vectors defined by the place code, the barcode, and the seed code. Data were smoothed with a Gaussian window (length = 250 ms, by convention σ = 47 ms). Activity was aligned separately to onsets and offsets of caches; median cache duration was 1.2 s. Error bars in all panels: SEM.

See also Figure S7.

holding out one check at a time when computing the seed vector. Seed responses diverged between occupied and empty checks ~100 ms after the bird lifted the cover flap and peaked just after check offset (Figure 7B). The seed response was absent when the chickadee visited a site without checking (Figures 7C and 7D).

The seed response was strong not only during occupied checks but also during caches (Figures 7E and S7). In population activity and in single-cell firing, this response was tightly locked to the offset of the cache—i.e., the moment when the chickadee left a seed in the site. The seed response was not as strong beforehand in spite of the chickadee's having a prolonged interaction with the seed before leaving it in the site. The seed response thus seemed to occur only when the bird attended to a seed in a site, during both checks and caches.

We wondered how the time course of the seed response compared to other activity patterns. We projected population activity onto cross-validated place code and barcode vectors for each site. We found that the three responses followed different time courses (Figure 7F). The place code peaked prior to the cache, roughly when the chickadee arrived at the site. The barcode increased prior to the onset and peaked during the cache itself. The seed response peaked at the offset of the cache. Place, barcode, and seed projections showed similar timing during visits, checks, and retrievals, although the magnitudes of barcode and seed projections were smaller than during caches (Figure S7). Our results show a complex sequence of hippocampal responses during caching, synchronized with behavior on a sub-second timescale.

DISCUSSION

Our recordings reveal sparse patterns of hippocampal activity (barcodes) that uniquely represent food-caching events. We use the term "barcoding" by analogy with other examples in biology where unique labels are defined by a vector code, such as a sequence of nucleotides (DNA barcoding[58] and cellular barcoding[59]) or a set of powers across different wavelengths (spectral barcoding[60,61]). This term has therefore been applied to vectors that are binary, otherwise discrete valued, or even continuous valued—as in the case of firing rates across neurons in our study. Tagging of distinct events by unique identifiers is also analogous to "hash coding" in computer science.

Barcodes are a population vector code—a concept that includes many other examples, including the place code. We use the more specific term "barcode" to describe them because they differ from most other population vector codes in neuroscience. The most notable difference is that population vectors usually correlate to smooth, continuous features of the world, such as spatial location in the case of the place code. Throughout a

behavioral task, these vectors therefore occupy a low-dimensional manifold whose structure is related to the structure of the task itself.[11,62–64] Barcodes, on the other hand, are seemingly random and uncorrelated even between adjacent sites. The lack of a correlation structure implies that these codes are extremely high dimensional, with at least as many dimensions as there are cache sites. Another difference is that barcodes activate transiently, only for the brief time that it takes a chickadee to interact with a cache site, whereas the place code is active during all movement. Finally, barcodes are not stable representations of any variable, including location: they are different even across caches at the same site. These properties are instead consistent with a barcode's being a unique signature of a specific event.

A crucial observation is that cells participating in barcodes are not a specialized class of neurons. Although it is possible, using standard statistical thresholds, to quantify what fraction of cells participate in barcodes (~30%), this fraction represents an arbitrary end of a continuum and will increase as more caches are recorded. This is similar to the place code, for which the fraction of significant place cells (~50% in our study) is defined by an arbitrary threshold on a continuum of spatial selectivity. In addition, barcode and place code responses are fully mixed in the hippocampal population, with no evidence of clustering into "barcode cells" or "place cells." In other words, there is no relationship between an individual neuron's barcode activity and its place tuning.

There are many other examples of mixed selectivity in the hippocampus—i.e., the coding of both spatial location and other task variables by the same population of neurons.[5,7,9–11,14] This is often observed when hippocampal neurons modify their spatial representations ("remap") in response to changes of sensory stimuli or behavioral goals.[6,14,65–67] One difference from this phenomenon is that barcodes are site specific and discontinuous in space and therefore do not encode yet another smooth map of the environment. Rather, barcode firing seems to be a truly distinct state of hippocampal activity, with an increased level of inhibition and a sparsification of neural responses. Switching between place coding and barcoding is therefore different from the conventional remapping between two smooth spatial representations. Finally, barcodes are different even for caches at the same location. Therefore, they cannot be easily explained by conjunctive coding of spatial location with other task variables.

Many studies have shown that experience can modify the firing of place cells. For example, place maps of different environments gradually diverge as an animal spends time exploring these environments.[19] Place fields also reorganize to overrepresent rewards and other salient locations.[17,20,54,68] Changes to place fields can even be sudden, suggesting a capacity for rapid learning.[22,23,69–71] In contrast to these studies, we have not observed changes to the place code resulting from food-caching events. This finding implies a dissociation of hippocampal mechanisms for different types of memory. Acquired knowledge about consistent features of an environment may be represented by the place code. In contrast, specific events within that environment appear to be represented by barcodes.

Our work parallels ideas about episodic memory from other systems. In the human hippocampus, activity patterns that occur during memory formation reactivate during episodic recall.[26,72–75] It is generally assumed that reactivated neurons are tuned to specific components of the memory. For instance, a neuron responsive to a specific object in a movie scene may fire when a person describes that object later in time. Recent work, however, found that some hippocampal neurons represent specific episodes (e.g., several objects occurring together in a scene) without responding separately to the individual components of those episodes.[26] This event-specific activity may be similar to the chickadee barcodes.

In animal models, the concept of an "engram" is often used to describe cells that represent a memory.[76,77] As with the human data, there is an ongoing inquiry into the nature of engrams. In the traditional definition, an engram includes all cells that reactivate between memory formation and recall. In our data, these cells would include not only the barcode but also place cells and seed-responsive cells. More recent studies have proposed treating cells that were already active before a memory (such as place cells) separately from those that become newly active during memory formation.[27,28] Our findings are consistent with barcodes being engrams in this updated definition.

Overall, our data provide no evidence that barcodes are unique to chickadees. Rather, some features of the food-caching behavior might have simply made these patterns detectable in the neural data. These behavioral features include exceptionally large numbers of memory storage and recall events that occur at well-defined locations and moments in time. It may be possible, in both human and animal models, to design behavioral tasks that offer some of the same advantages. Rodents and bats, for example, excel at spatial memory, exhibit single-shot learning that resembles avian cache memory,[20] and show hippocampal responses to brief, salient events.[67,78]

Our analysis shows a precise temporal coordination of the barcodes with the place code and the seed code. During a caching event, these codes occur within a window of ~1 s, compatible with known mechanisms of fast hippocampal plasticity.[70,71,79] It is conceivable that a similar mechanism in birds synaptically links neurons that participate in these codes. One idea is that during memory formation, neurons involved in the barcode connect with place cells and seed-responsive cells, in effect linking representations of place and food. In this model, barcodes bind different components of memory but prevent interference that would arise if, for example, many place cells directly linked to the same neuron representing a sunflower seed. As a result of this binding, partial reactivation of place or seed inputs—e.g., when a bird is searching for a nearby cache—could reactivate the barcode. This idea is consistent with the theory that hippocampal neurons encode an index that binds inputs active during an episode.[24–26]

Our results make it tempting to conclude that barcode reactivation is a mechanism of memory recall. We have not shown this to be generally the case. Reactivation during checks and retrievals happens when the chickadee is already at a cache site, about to open the cover flap. However, memory recall does not happen only locally but should also happen in advance when a chickadee decides where to travel next. Such remote

recall is especially important for an animal navigating through a large natural environment that is sparsely populated by caches. To be a mechanism of remote recall, barcodes should activate whenever birds make navigational choices that are guided by cache memories. This prediction remains to be tested in future work.

Limitations of the study

A major question is to what extent our results will generalize to other forms of episodic memory. Food caches are relatively simple events that occur at single moments in time. Episodic memory, however, can reference multiple temporally linked events and recall them in an entire sequence.[1] Neural signals in our study have also been analyzed across a relatively short timescale of ~1 h, which is in the range of intermediate-term memory.[80] Episodic memories, in contrast, are often stored long term and can last a lifetime. Even chickadees have been shown to remember caches for up to a month[36] in spite of typically retrieving food within several hours.[29] We do not know if barcodes are used in these more general conditions or whether they interact with other hippocampal mechanisms of episodic memory. Finally, our results do not speak to the cellular or synaptic mechanisms of memory storage. Although some aspects of neural dynamics have allowed us to speculate about these mechanisms, the barcodes remain a phenomenological observation about the properties of hippocampal activity.

STAR★METHODS

Detailed methods are provided in the online version of this paper and include the following:

- KEY RESOURCES TABLE
- RESOURCE AVAILABILITY
  - Lead contact
  - Materials availability
  - Data and code availability
- EXPERIMENTAL MODEL AND STUDY PARTICIPANT DETAILS
- METHOD DETAILS
  - 2D arena design
  - Behavioral protocol
  - Postural tracking
  - Action identification and neural window definitions
  - Detection of caching and retrieval
  - Design of the electrophysiology implant
  - Surgical approach
  - Electrophysiology protocol and spiking data preprocessing
  - Population firing rate deviation
  - Single-neuron place and cache tuning
  - Population vector correlation-based analyses
  - Place code subtraction
  - 1D behavior on a circular track
  - Calcium imaging
  - Analysis of calcium imaging data
  - Effects of caching on the place code
  - Seed tuning
  - Population projections of place code, barcode, and seed code
  - Histology
- QUANTIFICATION AND STATISTICAL ANALYSIS

SUPPLEMENTAL INFORMATION

Supplemental information can be found online at https://doi.org/10.1016/j.cell.2024.02.032.

ACKNOWLEDGMENTS

We thank D. Biderman and L. Paninski for help with pose-tracking methods; H. Payne for contributions to developing electrophysiology techniques; L. Abbott and A. Williams for advice and discussions; the Black Rock Forest Consortium, J. Scribner and the Hickory Hill Farm, and T. Green for help with fieldwork; and members of the Aronov laboratory for comments on the manuscript. Illustrations in Figure 1A are by J. Kuhl. This research was supported by the Beckman Foundation Young Investigator Award, the New York Stem Cell Foundation Robertson Neuroscience Investigator Award, the NIH Director's New Innovator Award (DP2-AG071918), the NIH BRAIN Initiative Postdoctoral Fellowship (S.N.C., 5F32MH123015), the Simons Society of Fellows (E.L.M.), and the NIH Pathway to Independence Award (E.L.M., 1K99NS121256).

AUTHOR CONTRIBUTIONS

S.N.C., E.L.M., and D.A. conceived the study. S.N.C. performed and analyzed behavioral and electrophysiology experiments and developed methods for 3D tracking. E.L.M. performed and analyzed calcium imaging experiments. S.H. acquired animals and assisted with animal care, data analysis, and experiments. S.N.C. and D.A. wrote the manuscript. D.A. supervised the project.

DECLARATION OF INTERESTS

The authors declare no competing interests.

Received: July 18, 2023
Revised: November 28, 2023
Accepted: February 23, 2024
Published: March 29, 2024

REFERENCES

1. Tulving, E., and Donaldson, W. (1972). Organization of Memory, Second Edition (Academic Press).
2. Vargha-Khadem, F., Gadian, D.G., Watkins, K.E., Connelly, A., Van Paesschen, W., and Mishkin, M. (1997). Differential Effects of Early Hippocampal Pathology on Episodic and Semantic Memory. Science *277*, 376–380. https://doi.org/10.1126/science.277.5324.376.
3. Scoville, W.B., and Milner, B. (1957). Loss of recent memory after bilateral hippocampal lesions. J. Neurol. Neurosurg. Psychiatry *20*, 11–21.
4. O'Keefe, J., and Dostrovsky, J. (1971). The hippocampus as a spatial map. Preliminary evidence from unit activity in the freely-moving rat. Brain Res. *34*, 171–175. https://doi.org/10.1016/0006-8993(71)90358-1.
5. Anderson, M.I., and Jeffery, K.J. (2003). Heterogeneous Modulation of Place Cell Firing by Changes in Context. J. Neurosci. *23*, 8827–8835. https://doi.org/10.1523/JNEUROSCI.23-26-08827.2003.
6. Muller, R.U., and Kubie, J.L. (1987). The effects of changes in the environment on the spatial firing of hippocampal complex-spike cells. J. Neurosci. *7*, 1951–1968. https://doi.org/10.1523/JNEUROSCI.07-07-01951.1987.
7. Leutgeb, S., Leutgeb, J.K., Barnes, C.A., Moser, E.I., McNaughton, B.L., and Moser, M.-B. (2005). Independent codes for spatial and episodic

memory in hippocampal neuronal ensembles. Science *309*, 619–623. https://doi.org/10.1126/science.1114037.

8. MacDonald, C.J., Carrow, S., Place, R., and Eichenbaum, H. (2013). Distinct Hippocampal Time Cell Sequences Represent Odor Memories in Immobilized Rats. J. Neurosci. *33*, 14607–14616. https://doi.org/10.1523/JNEUROSCI.1537-13.2013.
9. Frank, L.M., Brown, E.N., and Wilson, M. (2000). Trajectory encoding in the hippocampus and entorhinal cortex. Neuron *27*, 169–178. https://doi.org/10.1016/s0896-6273(00)00018-0.
10. Wood, E.R., Dudchenko, P.A., Robitsek, R.J., and Eichenbaum, H. (2000). Hippocampal neurons encode information about different types of memory episodes occurring in the same location. Neuron *27*, 623–633. https://doi.org/10.1016/s0896-6273(00)00071-4.
11. Aronov, D., Nevers, R., and Tank, D.W. (2017). Mapping of a non-spatial dimension by the hippocampal–entorhinal circuit. Nature *543*, 719–722. https://doi.org/10.1038/nature21692.
12. Pastalkova, E., Itskov, V., Amarasingham, A., and Buzsáki, G. (2008). Internally Generated Cell Assembly Sequences in the Rat Hippocampus. Science *321*, 1322–1327. https://doi.org/10.1126/science.1159775.
13. Manns, J.R., Howard, M.W., and Eichenbaum, H. (2007). Gradual Changes in Hippocampal Activity Support Remembering the Order of Events. Neuron *56*, 530–540. https://doi.org/10.1016/j.neuron.2007.08.017.
14. Colgin, L.L., Moser, E.I., and Moser, M.-B. (2008). Understanding memory through hippocampal remapping. Trends Neurosci. *31*, 469–477. https://doi.org/10.1016/j.tins.2008.06.008.
15. Widloski, J., and Foster, D.J. (2022). Flexible rerouting of hippocampal replay sequences around changing barriers in the absence of global place field remapping. Neuron *110*, 1547–1558.e8. https://doi.org/10.1016/j.neuron.2022.02.002.
16. Bostock, E., Muller, R.U., and Kubie, J.L. (1991). Experience-dependent modifications of hippocampal place cell firing. Hippocampus *1*, 193–205. https://doi.org/10.1002/hipo.450010207.
17. Hollup, S.A., Molden, S., Donnett, J.G., Moser, M.-B., and Moser, E.I. (2001). Accumulation of Hippocampal Place Fields at the Goal Location in an Annular Watermaze Task. J. Neurosci. *21*, 1635–1644. https://doi.org/10.1523/JNEUROSCI.21-05-01635.2001.
18. Kentros, C.G., Agnihotri, N.T., Streater, S., Hawkins, R.D., and Kandel, E.R. (2004). Increased Attention to Spatial Context Increases Both Place Field Stability and Spatial Memory. Neuron *42*, 283–295. https://doi.org/10.1016/S0896-6273(04)00192-8.
19. Lever, C., Wills, T., Cacucci, F., Burgess, N., and O'Keefe, J. (2002). Long-term plasticity in hippocampal place-cell representation of environmental geometry. Nature *416*, 90–94. https://doi.org/10.1038/416090a.
20. Dupret, D., O'Neill, J., Pleydell-Bouverie, B., and Csicsvari, J. (2010). The reorganization and reactivation of hippocampal maps predict spatial memory performance. Nat. Neurosci. *13*, 995–1002. https://doi.org/10.1038/nn.2599.
21. McKenzie, S., Frank, A.J., Kinsky, N.R., Porter, B., Rivière, P.D., and Eichenbaum, H. (2014). Hippocampal Representation of Related and Opposing Memories Develop within Distinct, Hierarchically Organized Neural Schemas. Neuron *83*, 202–215. https://doi.org/10.1016/j.neuron.2014.05.019.
22. Moita, M.A.P., Rosis, S., Zhou, Y., LeDoux, J.E., and Blair, H.T. (2004). Putting fear in its place: remapping of hippocampal place cells during fear conditioning. J. Neurosci. *24*, 7015–7023. https://doi.org/10.1523/JNEUROSCI.5492-03.2004.
23. Frank, L.M., Stanley, G.B., and Brown, E.N. (2004). Hippocampal Plasticity across Multiple Days of Exposure to Novel Environments. J. Neurosci. *24*, 7681–7689. https://doi.org/10.1523/JNEUROSCI.1958-04.2004.
24. Teyler, T.J., and DiScenna, P. (1986). The hippocampal memory indexing theory. Behav. Neurosci. *100*, 147–154. https://doi.org/10.1037/0735-7044.100.2.147.
25. Teyler, T.J., and Rudy, J.W. (2007). The hippocampal indexing theory and episodic memory: updating the index. Hippocampus *17*, 1158–1169. https://doi.org/10.1002/hipo.20350.
26. Kolibius, L.D., Roux, F., Parish, G., Ter Wal, M., Van Der Plas, M., Chelvarajah, R., Sawlani, V., Rollings, D.T., Lang, J.D., Gollwitzer, S., et al. (2023). Hippocampal neurons code individual episodic memories in humans. Nat. Hum. Behav. *7*, 1968–1979. https://doi.org/10.1038/s41562-023-01706-6.
27. Tanaka, K.Z., He, H., Tomar, A., Niisato, K., Huang, A.J.Y., and McHugh, T.J. (2018). The hippocampal engram maps experience but not place. Science *361*, 392–397. https://doi.org/10.1126/science.aat5397.
28. Goode, T.D., Tanaka, K.Z., Sahay, A., and McHugh, T.J. (2020). An Integrated Index: Engrams, Place Cells, and Hippocampal Memory. Neuron *107*, 805–820. https://doi.org/10.1016/j.neuron.2020.07.011.
29. Cowie, R.J., Krebs, J.R., and Sherry, D.F. (1981). Food storing by marsh tits. Anim. Behav. *29*, 1252–1259. https://doi.org/10.1016/S0003-3472(81)80077-2.
30. Pravosudov, V.V. (1985). Food searching and storing by *Parus cinctus lapponicus* and *Parus montanus borealis* (Paridae). Zool. Zhurnal *64*, 1036–1043.
31. Stevens, T.A., and Krebs, J.R. (1986). Retrieval of stored seeds by Marsh Tits *Parus palustris* in the field. Ibis *128*, 513–525. https://doi.org/10.1111/j.1474-919X.1986.tb02703.x.
32. Sherry, D.F., Krebs, J.R., and Cowie, R.J. (1981). Memory for the location of stored food in marsh tits. Anim. Behav. *29*, 1260–1266. https://doi.org/10.1016/S0003-3472(81)80078-4.
33. Sherry, D. (1984). Food storage by black-capped chickadees: Memory for the location and contents of caches. Anim. Behav. *32*, 451–464. https://doi.org/10.1016/S0003-3472(84)80281-X.
34. Applegate, M.C., and Aronov, D. (2022). Flexible use of memory by food-caching birds. eLife *11*, e70600. https://doi.org/10.7554/eLife.70600.
35. Herz, R.S., Zanette, L., and Sherry, D.F. (1994). Spatial cues for cache retrieval by black-capped chickadees. Anim. Behav. *48*, 343–351. https://doi.org/10.1006/anbe.1994.1247.
36. Hitchcock, C.L., and Sherry, D.F. (1990). Long-term memory for cache sites in the black-capped chickadee. Anim. Behav. *40*, 701–712. https://doi.org/10.1016/S0003-3472(05)80699-2.
37. Brodin, A. (1993). Radio-Ptilochronology: Tracing Radioactively Labelled Food in Feathers. Ornis Scand. *24*, 167–173. https://doi.org/10.2307/3676732.
38. Feeney, M.C., Roberts, W.A., and Sherry, D.F. (2011). Mechanisms of what-where-when memory in black-capped chickadees (*Poecile atricapillus*): Do chickadees remember "when"? J. Comp. Psychol. *125*, 308–316. https://doi.org/10.1037/a0023635.
39. Clayton, N.S., and Dickinson, A. (1998). Episodic-like memory during cache recovery by scrub jays. Nature *395*, 272–274. https://doi.org/10.1038/26216.
40. Salwiczek, L.H., Watanabe, A., and Clayton, N.S. (2010). Ten years of research into avian models of episodic-like memory and its implications for developmental and comparative cognition. Behav. Brain Res. *215*, 221–234. https://doi.org/10.1016/j.bbr.2010.06.011.
41. DeVito, L.M., and Eichenbaum, H. (2010). Distinct contributions of the hippocampus and medial prefrontal cortex to the "what–where–when" components of episodic-like memory in mice. Behav. Brain Res. *215*, 318–325. https://doi.org/10.1016/j.bbr.2009.09.014.
42. Sherry, D.F., and Vaccarino, A.L. (1989). Hippocampus and memory for food caches in black-capped chickadees. Behav. Neurosci. *103*, 308–318. https://doi.org/10.1037/0735-7044.103.2.308.
43. Krushinskaya, N.L. (1966). Some complex forms of feeding behaviour of nutcracker *Nucifraga caryocatactes*, after removal of old cortex. Zh. Evol. Biochim. Fisiol. *11*, 563–568.
44. Abellán, A., Desfilis, E., and Medina, L. (2014). Combinatorial expression of *Lef1*, *Lhx2*, *Lhx5*, *Lhx9*, *Lmo3*, *Lmo4*, and *Prox1* helps to identify

comparable subdivisions in the developing hippocampal formation of mouse and chicken. Front. Neuroanat. *8*, 59. https://doi.org/10.3389/fnana.2014.00059.

45. Tosches, M.A., Yamawaki, T.M., Naumann, R.K., Jacobi, A.A., Tushev, G., and Laurent, G. (2018). Evolution of pallium, hippocampus, and cortical cell types revealed by single-cell transcriptomics in reptiles. Science *360*, 881–888. https://doi.org/10.1126/science.aar4237.
46. Sherry, D.F., Vaccarino, A.L., Buckenham, K., and Herz, R.S. (1989). The Hippocampal Complex of Food-Storing Birds. Brain Behav. Evol. *34*, 308–317. https://doi.org/10.1159/000116516.
47. Krebs, J.R., Sherry, D.F., Healy, S.D., Perry, V.H., and Vaccarino, A.L. (1989). Hippocampal specialization of food-storing birds. Proc. Natl. Acad. Sci. USA *86*, 1388–1392.
48. Payne, H.L., Lynch, G.F., and Aronov, D. (2021). Neural representations of space in the hippocampus of a food-caching bird. Science *373*, 343–348. https://doi.org/10.1126/science.abg2009.
49. Agarwal, A., Sarel, A., Derdikman, D., Ulanovsky, N., and Gutfreund, Y. (2023). Spatial coding in the hippocampus and hyperpallium of flying owls. Proc. Natl. Acad. Sci. USA *120*, e2212418120. https://doi.org/10.1073/pnas.2212418120.
50. Applegate, M.C., Gutnichenko, K.S., Mackevicius, E.L., and Aronov, D. (2023). An entorhinal-like region in food-caching birds. Curr. Biol. *33*, 2465–2477.e7. https://doi.org/10.1016/j.cub.2023.05.031.
51. Pravosudov, V.V., and Grubb, T.C. (1997). Management of fat reserves and food caches in tufted titmice (*Parus bicolor*) in relation to unpredictable food supply. Behav. Ecol. *8*, 332–339. https://doi.org/10.1093/beheco/8.3.332.
52. Ahmed, O.J., and Mehta, M.R. (2009). The hippocampal rate code: anatomy, physiology and theory. Trends Neurosci. *32*, 329–338. https://doi.org/10.1016/j.tins.2009.01.009.
53. Buzsáki, G. (2015). Hippocampal sharp wave-ripple: A cognitive biomarker for episodic memory and planning. Hippocampus *25*, 1073–1188. https://doi.org/10.1002/hipo.22488.
54. Gauthier, J.L., and Tank, D.W. (2018). A Dedicated Population for Reward Coding in the Hippocampus. Neuron *99*, 179–193.e7. https://doi.org/10.1016/j.neuron.2018.06.008.
55. Mehta, M.R., Barnes, C.A., and McNaughton, B.L. (1997). Experience-dependent, asymmetric expansion of hippocampal place fields. Proc. Natl. Acad. Sci. USA *94*, 8918–8921. https://doi.org/10.1073/pnas.94.16.8918.
56. Nakazawa, K., Sun, L.D., Quirk, M.C., Rondi-Reig, L., Wilson, M.A., and Tonegawa, S. (2003). Hippocampal CA3 NMDA Receptors Are Crucial for Memory Acquisition of One-Time Experience. Neuron *38*, 305–315. https://doi.org/10.1016/S0896-6273(03)00165-X.
57. Mehta, M.R., Quirk, M.C., and Wilson, M.A. (2000). Experience-Dependent Asymmetric Shape of Hippocampal Receptive Fields. Neuron *25*, 707–715. https://doi.org/10.1016/S0896-6273(00)81072-7.
58. Hebert, P.D.N., Ratnasingham, S., and deWaard, J.R. (2003). Barcoding animal life: cytochrome c oxidase subunit 1 divergences among closely related species. Proc. Biol. Sci. *270* (*Suppl 1*), S96–S99. https://doi.org/10.1098/rsbl.2003.0025.
59. Kebschull, J.M., and Zador, A.M. (2018). Cellular barcoding: lineage tracing, screening and beyond. Nat. Methods *15*, 871–879. https://doi.org/10.1038/s41592-018-0185-x.
60. Lubeck, E., and Cai, L. (2012). Single-cell systems biology by super-resolution imaging and combinatorial labeling. Nat. Methods *9*, 743–748. https://doi.org/10.1038/nmeth.2069.
61. Livet, J., Weissman, T.A., Kang, H., Draft, R.W., Lu, J., Bennis, R.A., Sanes, J.R., and Lichtman, J.W. (2007). Transgenic strategies for combinatorial expression of fluorescent proteins in the nervous system. Nature *450*, 56–62. https://doi.org/10.1038/nature06293.
62. Russo, A.A., Bittner, S.R., Perkins, S.M., Seely, J.S., London, B.M., Lara, A.H., Miri, A., Marshall, N.J., Kohn, A., Jessell, T.M., et al. (2018). Motor Cortex Embeds Muscle-like Commands in an Untangled Population Response. Neuron *97*, 953–966.e8. https://doi.org/10.1016/j.neuron.2018.01.004.
63. Nieh, E.H., Schottdorf, M., Freeman, N.W., Low, R.J., Lewallen, S., Koay, S.A., Pinto, L., Gauthier, J.L., Brody, C.D., and Tank, D.W. (2021). Geometry of abstract learned knowledge in the hippocampus. Nature *595*, 80–84. https://doi.org/10.1038/s41586-021-03652-7.
64. Gardner, R.J., Hermansen, E., Pachitariu, M., Burak, Y., Baas, N.A., Dunn, B.A., Moser, M.-B., and Moser, E.I. (2022). Toroidal topology of population activity in grid cells. Nature *602*, 123–128. https://doi.org/10.1038/s41586-021-04268-7.
65. Kelemen, E., and Fenton, A.A. (2010). Dynamic grouping of hippocampal neural activity during cognitive control of two spatial frames. PLoS Biol. *8*, e1000403. https://doi.org/10.1371/journal.pbio.1000403.
66. Jezek, K., Henriksen, E.J., Treves, A., Moser, E.I., and Moser, M.-B. (2011). Theta-paced flickering between place-cell maps in the hippocampus. Nature *478*, 246–249. https://doi.org/10.1038/nature10439.
67. Sarel, A., Palgi, S., Blum, D., Aljadeff, J., Las, L., and Ulanovsky, N. (2022). Natural switches in behaviour rapidly modulate hippocampal coding. Nature *609*, 119–127. https://doi.org/10.1038/s41586-022-05112-2.
68. Hetherington, P.A., and Shapiro, M.L. (1997). Hippocampal place fields are altered by the removal of single visual cues in a distance-dependent manner. Behav. Neurosci. *111*, 20–34. https://doi.org/10.1037/0735-7044.111.1.20.
69. Monaco, J.D., Rao, G., Roth, E.D., and Knierim, J.J. (2014). Attentive scanning behavior drives one-trial potentiation of hippocampal place fields. Nat. Neurosci. *17*, 725–731. https://doi.org/10.1038/nn.3687.
70. Bittner, K.C., Milstein, A.D., Grienberger, C., Romani, S., and Magee, J.C. (2017). Behavioral time scale synaptic plasticity underlies CA1 place fields. Science *357*, 1033–1036. https://doi.org/10.1126/science.aan3846.
71. Sheffield, M.E.J., Adoff, M.D., and Dombeck, D.A. (2017). Increased Prevalence of Calcium Transients across the Dendritic Arbor during Place Field Formation. Neuron *96*, 490–504.e5. https://doi.org/10.1016/j.neuron.2017.09.029.
72. Gelbard-Sagiv, H., Mukamel, R., Harel, M., Malach, R., and Fried, I. (2008). Internally Generated Reactivation of Single Neurons in Human Hippocampus During Free Recall. Science *322*, 96–101. https://doi.org/10.1126/science.1164685.
73. Manning, J.R., Polyn, S.M., Baltuch, G.H., Litt, B., and Kahana, M.J. (2011). Oscillatory patterns in temporal lobe reveal context reinstatement during memory search. Proc. Natl. Acad. Sci. USA *108*, 12893–12897. https://doi.org/10.1073/pnas.1015174108.
74. Tompary, A., Duncan, K., and Davachi, L. (2016). High-resolution investigation of memory-specific reinstatement in the hippocampus and perirhinal cortex. Hippocampus *26*, 995–1007. https://doi.org/10.1002/hipo.22582.
75. Chadwick, M.J., Hassabis, D., Weiskopf, N., and Maguire, E.A. (2010). Decoding Individual Episodic Memory Traces in the Human Hippocampus. Curr. Biol. *20*, 544–547. https://doi.org/10.1016/j.cub.2010.01.053.
76. Liu, X., Ramirez, S., Pang, P.T., Puryear, C.B., Govindarajan, A., Deisseroth, K., and Tonegawa, S. (2012). Optogenetic stimulation of a hippocampal engram activates fear memory recall. Nature *484*, 381–385. https://doi.org/10.1038/nature11028.
77. Tonegawa, S., Liu, X., Ramirez, S., and Redondo, R. (2015). Memory Engram Cells Have Come of Age. Neuron *87*, 918–931. https://doi.org/10.1016/j.neuron.2015.08.002.
78. Green, L., Tingley, D., Rinzel, J., and Buzsáki, G. (2022). Action-driven remapping of hippocampal neuronal populations in jumping rats. Proc. Natl. Acad. Sci. USA *119*, e2122141119. https://doi.org/10.1073/pnas.2122141119.
79. Milstein, A.D., Li, Y., Bittner, K.C., Grienberger, C., Soltesz, I., Magee, J.C., and Romani, S. (2021). Bidirectional synaptic plasticity rapidly modifies

hippocampal representations. eLife *10*, e73046. https://doi.org/10.7554/eLife.73046.

80. Kandel, E.R., Dudai, Y., and Mayford, M.R. (2014). The Molecular and Systems Biology of Memory. Cell *157*, 163–186. https://doi.org/10.1016/j.cell.2014.03.001.
81. Chen, T.-W., Wardill, T.J., Sun, Y., Pulver, S.R., Renninger, S.L., Baohan, A., Schreiter, E.R., Kerr, R.A., Orger, M.B., Jayaraman, V., et al. (2013). Ultrasensitive fluorescent proteins for imaging neuronal activity. Nature *499*, 295–300. https://doi.org/10.1038/nature12354.
82. Graving, J.M., Chae, D., Naik, H., Li, L., Koger, B., Costelloe, B.R., and Couzin, I.D. (2019). DeepPoseKit, a software toolkit for fast and robust animal pose estimation using deep learning. eLife *8*, e47994. https://doi.org/10.7554/eLife.47994.
83. Abadi, M., Agarwal, A., Barham, P., Brevdo, E., Chen, Z., Citro, C., Corrado, G.S., Davis, A., Dean, J., Devin, M., et al. (2016). TensorFlow: Large-Scale Machine Learning on Heterogeneous Distributed Systems. Preprint at arXiv. https://arxiv.org/abs/1603.04467.
84. Pachitariu, M., Steinmetz, N.A., Kadir, S.N., Carandini, M., and Harris, K.D. (2016). Fast and Accurate Spike Sorting of High-Channel Count Probes with KiloSort. Adv. Neural Inf. Process. Syst. *29*, 4448–4456.
85. Zhou, P., Resendez, S.L., Rodriguez-Romaguera, J., Jimenez, J.C., Neufeld, S.Q., Giovannucci, A., Friedrich, J., Pnevmatikakis, E.A., Stuber, G.D., Hen, R., et al. (2018). Efficient and accurate extraction of in vivo calcium signals from microendoscopic video data. eLife *7*, e28728. https://doi.org/10.7554/eLife.28728.
86. Dunn, T.W., Marshall, J.D., Severson, K.S., Aldarondo, D.E., Hildebrand, D.G.C., Chettih, S.N., Wang, W.L., Gellis, A.J., Carlson, D.E., Aronov, D., et al. (2021). Geometric deep learning enables 3D kinematic profiling across species and environments. Nat. Methods *18*, 564–573. https://doi.org/10.1038/s41592-021-01106-6.
87. Skaggs, W., McNaughton, B., and Gothard, K. (1992). An Information-Theoretic Approach to Deciphering the Hippocampal Code. Adv. Neural Inf. Process. Syst. *5*, 1030–1037.
88. Markus, E.J., Barnes, C.A., McNaughton, B.L., Gladden, V.L., and Skaggs, W.E. (1994). Spatial information content and reliability of hippocampal CA1 neurons: Effects of visual input. Hippocampus *4*, 410–421. https://doi.org/10.1002/hipo.450040404.
89. Nath, T., Mathis, A., Chen, A.C., Patel, A., Bethge, M., and Mathis, M.W. (2019). Using DeepLabCut for 3D markerless pose estimation across species and behaviors. Nat. Protoc. *14*, 2152–2176. https://doi.org/10.1038/s41596-019-0176-0.
90. Mott, R., Herrod, A., Hodgson, J.C., and Clarke, R.H. (2015). An Evaluation of the Use of Predicted Harness Spans for Correctly Fitting Leg-Loop Harnesses in Seabird Research. Waterbirds *38*, 420–424.
91. Mackevicius, E.L., Gu, S., Denisenko, N.I., and Fee, M.S. (2023). Self-organization of songbird neural sequences during social isolation. eLife *12*, e77262. https://doi.org/10.7554/eLife.77262.
92. Friedrich, J., Yang, W., Soudry, D., Mu, Y., Ahrens, M.B., Yuste, R., Peterka, D.S., and Paninski, L. (2017). Multi-scale approaches for high-speed imaging and analysis of large neural populations. PLoS Comput. Biol. *13*, e1005685. https://doi.org/10.1371/journal.pcbi.1005685.
93. Chettih, S.N., and Harvey, C.D. (2019). Single-neuron perturbations reveal feature-specific competition in V1. Nature *567*, 334–340. https://doi.org/10.1038/s41586-019-0997-6.
94. Guizar-Sicairos, M., Thurman, S.T., and Fienup, J.R. (2008). Efficient subpixel image registration algorithms. Opt. Lett. *33*, 156–158. https://doi.org/10.1364/OL.33.000156.

STAR★METHODS

KEY RESOURCES TABLE

REAGENT or RESOURCE	SOURCE	IDENTIFIER
Bacterial and virus strains		
AAV9-pAAV.CAG.GCaMP6f.WPRE.SV40	Chen et al.[81]	Addgene plasmid #100836
Chemicals, peptides, and recombinant proteins		
4′,6-diamidino-2-phenylindole, dihydrochloride (DAPI)	Fischer Scientific	PI62247
Paraformaldehyde	Electron Microscopy Sciences	15710
Critical commercial assays		
nVista System	Inscopix	N/A
3D printer	Formlabs	Formlabs 3
Cameras	Blackfly	BFS-U3-70S7M-C
64-channel silicon probe	Cambridge NeuroTech	H6 ASSY-236
Nanodrive	Cambridge NeuroTech	Nanodrive
64-channel amplifier	Intan Technologies	RHD2164
Recording system	Intan Technologies	C3100
Motorized commutator	Doric Lenses	24_PZN12
Deposited data		
Behavioral data (postural tracking)	This paper	Dryad (https://doi.org/10.5061/dryad.7h44j101z)
Electrophysiology data	This paper	Dryad (https://doi.org/10.5061/dryad.7h44j101z)
Experimental models: Organisms/strains		
Poecile atricapillus (black-capped chickadee)	Wild-caught	N/A
Software and algorithms		
MATLAB 2020b	Mathworks	www.mathworks.com
Arduino	Open-source	www.arduino.cc
Inventor	Autodesk	www.autodesk.com
PIMAQ video acquisition software	Open-source	github.com/jbohnslav/PIMAQ
Laser pointer calibration software	Open-source	github.com/JohnsonLabJanelia/laserCalib
DeepPoseKit	Graving et al.[82]	N/A
TensorFlow	Abadi et al.[83]	N/A
Label 3D software	Open-source	github.com/diegoaldarondo/Label3D
Kilosort	Pachitariu et al.[84]	N/A
CNMF_E	Zhou et al.[85]	N/A

RESOURCE AVAILABILITY

Lead contact

Further information and requests for resources and reagents should be directed to and will be fulfilled by the lead contact, Dmitriy Aronov (da2006@columbia.edu).

Materials availability

This study did not generate new unique reagents.

Data and code availability

- Processed data have been deposited on Dryad and are publicly available as of the date of publication. DOIs are listed in the key resources table. Raw data will be shared by the lead contact upon request.
- Original code has been deposited on Dryad and is publicly available as of the date of publication. DOIs are listed in the key resources table.
- Any additional information required to reanalyze the data reported in this paper is available from the lead contact upon request.

EXPERIMENTAL MODEL AND STUDY PARTICIPANT DETAILS

All animal procedures were carried out following US National Institutes of Health guidelines, and approved by the Columbia University Institutional Animal Care and Use Committee. Five black-capped chickadees (three male, two female) were used for electrophysiological experiments in the 2D arena, and seven chickadees (one male, four female, two undetermined) were used for calcium imaging experiments on the circular track. Subjects were collected from multiple sites in New York State using Federal and State scientific collection licenses. Chickadees are not clearly sexually dimorphic, and all experiments were performed blindly to sex. Subject age at collection time was not precisely determined. Birds were collected between October and February, and data were acquired between three months and one year after collection. Birds were housed in groups of 1–3 on a "winter" light cycle (9:15 light:dark hours) before experiments began.

METHOD DETAILS

2D arena design

The arena for 2D behavior and electrophysiology was adapted from a previously published design.[34] It was designed in Autodesk Inventor and constructed from five layers of laser-cut material. The top layer was a 1.5 mm thick matte white acrylic sheet. The 2nd layer was 1/32″ thick 60A durometer synthetic rubber sheet. The 3rd layer was a 1 mm thick clear acrylic sheet. The 4th layer was a 5.6 mm thick black acrylic sheet. The bottom, 5th layer was a clear 1/8″ thick acrylic sheet. Wooden dowels 3/8″ in diameter and 1.5″ long were used for perches. Perches were aligned with slots laser-cut through all layers of the arena, and were secured using Loctite Fun-Tak. Cache sites were formed by a 0.3 x 0.25″ hole cut into the 4th arena layer, with the 5th layer forming a transparent bottom. The 2nd arena layer was cut to form a rubber flap which fully covered the underlying cache site, and the 1st arena layer was cut to allow access to the underlying rubber flap. The 3rd arena layer served as a spacer between the rubber flap and the 4th arena layer, in order to allow the bird to easily grab the flap with its beak.

The arena was designed as 4 symmetric quadrants, each containing 32 cache sites with one perch per site. Sites were positioned such that the midpoints between the centers of the sites and their matched perches lay on a 6x6 rectangular grid with 5.3 cm spacing. Sites were grouped in modules of 4 sites facing each cardinal direction. Four sites at the outside corner of each quadrant were eliminated to permit room for a feeder, resulting in a total of 128 cache sites. Feeders were constructed from 3D printed material (red, blue, green, and yellow Processed Versatile Plastic, Shapeways). A shallow dish holding sunflower seeds was covered by a top piece controlled by a stepper motor, allowing automated opening and closing of access to the dish beneath. The stepper motor was controlled by Arduino and a stepper motor driver. A perch was placed next to each of the feeders. Finally, a water dish was 3D printed (White Resin, Formlabs 3 printer) and inserted into a circular cutout in the center of the arena.

The entire arena was mounted on a custom-constructed aluminum frame. The frame also supported lighting and video cameras described below. A 6″ border constructed of matte white acrylic surrounded the arena and was also enclosed within the frame. Arena walls were constructed from white vinyl shower curtains cut to size and secured to the external frame. A single orienting cue (11 x 8″ black rectangle) was positioned in the center of one of the walls. Additional cues were 12 small stickers of varying colors and shapes placed on the floor of the arena in the space between arena quadrants.

Behavioral videos were collected using six Blackfly S cameras (BFS-U3-70S7M-C, Flir Teledyne, SONY IMX428 monochrome sensor) using wide-angle lenses (8 mm focal length, M111FM0-8, Tamron). Four of these cameras were positioned roughly at eye level with the chickadee in the corners of the arena. Two additional cameras were mounted on the ceiling (60 cm above the floor) at the midpoints of two opposite edges of the arena. Each of the six cameras was oriented to obtain a complete view of all the sites and feeders in the arena. We used 800 μs exposure times to minimize blur, and frame acquisition was synchronously triggered across all cameras at 60 Hz rate. We used PIMAQ software (https://github.com/jbohnslav/PIMAQ) to acquire video data. Videos were compressed online during acquisition to h.264 format using two NVidia RTX2080ti GPUs. Calibration for 3D registration of video data was performed using a laser pointer (https://github.com/JohnsonLabJanelia/laserCalib). A seventh camera was positioned beneath the arena in order to monitor the contents of cache sites. Frames of this camera were triggered synchronized with every other behavioral frame acquisition (i.e., at 30 Hz). The arena was illuminated by white LED panels (superbrightleds.com).

Behavioral protocol

At least one week before experiments, chickadees were transferred from colony to single housing. They were provided *ad-libitum* Mazuri small bird diet and weighed daily. Primary wing feathers were trimmed to prevent flight and promote ground foraging in the behavioral arena. A miniaturized assembly containing 4 cache sites identical to those used in the behavioral arena was baited with sunflower seeds and installed in the bird's home cage to permit familiarization with the cache site mechanism.

Before a chickadee woke on the morning of a behavioral experiment, all food was removed from its cage. The bird was food deprived and monitored regularly, typically for the first 3 h of the day. It was then placed in the behavioral arena. The arena contained a fresh water tray and four motorized feeders containing raw, shelled sunflower seeds chopped into halves. In a typical session, 6–8 cache sites were baited before the bird entered the arena. Feeders were closed for the initial 20 min and opened for 6 min every 50 min the bird remained in the arena. The exact duration of food-deprivation, number of initially baited sites, and precise feeder schedule were adjusted on a bird- and session-dependent basis, in order to optimize the bird's caching behavior and engagement

with the arena. Sessions were typically 120–180 min long. Birds were given at least one full day of rest with an *ad-libitum* food supply between experimental sessions.

Prior to any surgical manipulations, we ran behavioral habituation sessions. Many chickadees performed caching behavior in the arena during their initial exposure. Some birds required 2–4 behavioral sessions before readily caching and retrieving seeds, potentially due to the stress of handling and the novel environment, or unfamiliarity with the cache site mechanism. Behavioral habituation was continued until a bird appeared to comfortably perform caching behavior throughout a full session. A fraction of birds (~1/4) either did not exhibit motivation to cache, or did not engage with cache sites, and were excluded from further experiments. For included subjects, we excluded a small fraction of sessions where the bird performed under 30 caches during a session.

Postural tracking

Neural networks were used to track the animal's 3D posture during behavioral sessions. We used a custom implementation of a two-stage algorithm, inspired by the DANNCE algorithm,[86] and built using the DeepPoseKit framework[82] in TensorFlow 2.[83] The first stage of the algorithm consisted of a Stacked DenseNet, with two stacks and a growth rate of 40, which was trained to identify the coarse location of the bird's head, body, and tail in 4x spatially downsampled behavioral videos. The bird's body position in all 6 camera views was then used to triangulate 3D position, and the full-resolution video from each view was resampled and cropped such that the bird was centered and at constant physical scale. The second stage of the algorithm consisted of another Stacked DenseNet (2 stacks, growth rate 40) trained to detect 18 keypoints on the bird. Keypoints were chosen as reliably visually identifiable points on the bird's exterior that did not completely align to its underlying skeleton. These included the top and bottom tips of the beak, the top and back of its head, the centers of its back and front chest, and the base and tip of its tail. They also included the left and right eyes, lower corners of its bib marking, shoulders, ankles, and feet. The output of the second stage was the location and detection confidence of all of these 18 markers in all 6 camera views. Conversion from pixel to 3D coordinates was performed using standard triangulation techniques, for each frame utilizing all pairs of the four camera views with greatest confidence rankings for that frame, and taking the median across pairs.

Training data were prepared using Label 3D software (github.com/diegoaldarondo/Label3D). An initial set of 360 frames (or 2160 images using all 6 cameras) was manually annotated. The tracking algorithm was then run on new data, and new training data were iteratively selected using a consistency metric across views (the reprojection error) to identify postures with poor tracking performance. This procedure was continued until reprojection errors were ~1 pixel, after labeling 586 frames (3516 images). Accuracy was judged by subjectively evaluating videos, and by comparing predictions of the algorithm with two human annotators. Tracking was approximately as consistent with either annotator as the two were with each other (~1 mm positional difference). For analysis used in the paper, tracked coordinates were then post-processed using a Kalman filter to enforce smoothness, and to interpolate over rare, brief intervals where tracking was inconsistent across views (reprojection errors >12 pixels).

Action identification and neural window definitions

Continuous timeseries of 3D postural tracking data were parsed into a sequence of discrete actions. We first identified two kinds of events: movement between sites (i.e., the bird's feet landing on or leaving a perch), and interaction with a cache site (i.e., the tip of the beak coming into contact with the rubber flap covering the site).

We identified movement between sites by detecting "perch arrivals" and "perch departures". These were defined by determining when the chickadee's feet entered or exited a 2D bounding box surrounding each perch in the arena, excluding time points where the feet were moving rapidly (>20 cm/s). Chickadees rarely left one perch without hopping to a new perch. We identified cache site interactions by identifying periods when the bird's beak was within a 2D bounding box surrounding each cache site, and below a height threshold of 4 mm above the arena. If multiple interactions at the same site were identified within 1 s of each other, they were merged into a single longer-duration interaction.

For the analysis in this paper, actions were further subdivided into visits, checks, caches, and retrievals. These actions occurred in variable sequences and had different durations. For analysis of neural data aligned to these actions, we defined temporal windows that minimized bleed-through between them. We thus examined all perch arrivals, and identified if the bird made any interaction with the cache site before departure. Perch arrivals with no subsequent interaction of any kind were identified as "visits" in the main text. To define the window of the visit, we started with a window of ±500 ms from perch arrival, and then further refined this window to exclude confounding events. Specifically, the visit window was adjusted to begin after the offset of any interactions at other sites occurring before a visit at this site, and the visit window was truncated early if perch departure occurred less than 500 ms after arrival. Neural data during visits were defined by averaging neural activity within this window.

Caches and retrievals were defined as any cache site interactions resulting in the addition or removal of a seed, following procedures detailed in the next methods section. Caches and retrievals were extended events, typically lasting >1 s, with a heavy-tailed duration distribution. We defined a window starting 250 ms before the onset of an interaction, and extending 250 ms after the offset of the interaction. This window was further refined to start no earlier than departure from the previous perch, and to end no later than arrival at the next perch. Finally, the window for long site interactions (>2 s, ~5% of interactions) was adjusted to include only time periods up to 1 s after onset and up to 1 s before offset, excluding the times between. Neural data during caches and retrievals were defined by averaging neural activity within these windows.

The majority of each bird's site interactions were extremely brief, and involved a stereotyped motor program lasting 150–200 ms, during which the bird lifted the rubber flap with its beak and quickly peeked at site contents. We called these actions "checks". In order to ensure we were analyzing a highly stereotyped action, we used a Gaussian mixture model to classify postural timeseries aligned to site interaction onsets. Specifically, for all site interactions that were neither cache nor retrieval, we collected the following features derived from postural tracking: (1) height of the beak above the arena; (2) distance of the beak in the horizontal 2D plane from the center of the cache site; (3) the vertical angle of the head, determined by the vector between the midpoint of bird's eyes and the tip of its beak; (4) the distance of the beak tip from the bird's feet. We collected data for each feature as a 25-frame timeseries from −100 to +300 ms relative to interaction onset. We visualized the data using tSNE embeddings and manually defined the cluster of events in a dataset containing 47,913 site interactions taken from 3 sessions from each of the 5 birds used for electrophysiology. We also manually defined clusters for other less common site interaction such as long interactions, swiping the beak across the cache site, or touching cache sites which were not matched to the perch where the bird was positioned. A Gaussian mixture model was then defined by these features and manual labels, and used to classify all site manipulations in the dataset. Checks analyzed in the manuscript were defined as the vast majority of site interactions (excluding those with a cache or retrieval) classified as a stereotypical short check by the Gaussian mixture model. The other site interactions were excluded from analysis. The window used to average neural data for a check was from 250 ms before onset to 250 ms after offset. This window was further refined as for caches and retrievals to exclude overlap with movement between perches.

We examined alternative criteria for defining windows for each action, including windows ranging from 250 ms to 2 s wide aligned to event onsets. Results were not qualitatively affected by the choice of window.

Detection of caching and retrieval

In addition to tracking 3D posture, we developed neural networks for semi-automatically identifying the bird's seed handling, i.e., caching, retrieving, and other interactions with the cache site. We used video from the camera positioned below the arena, which could view the contents of cache sites through the transparent bottom. We cropped videos into 51x51 pixel bins centered on each cache site, and trained a neural network to predict whether each site was empty or occupied by at least one seed. The network consisted of layers with: 10 7 × 7 × 1 convolutions with stride 2, 25 3 × 3 × 10 convolutions with stride 1, 50 3 × 3 × 25 convolutions with stride 1, global average pooling, 25% dropout, and a 10 unit fully connected layer before a 2 unit softmax classification output. We applied ReLU activations, batch normalization, and 2x2 max pooling between layers. The classifications produced by this network were later cross-referenced using an algorithm described below.

We also built a variant of our two-stage postural tracking approach described above in order to identify when a bird was carrying a seed in its beak. This algorithm used the same first stage to coarsely track the bird's head, body and tail, and to triangulate 3D position. However rather than cropping around the body, for seed carrying detection we cropped a tighter region centered on the bird's face. A custom network implemented in TensorFlow 2[83] was then used to predict for each frame whether the bird currently held a seed in its beak. This network consisted of 25 7 × 7 × 1 convolutions with stride 2, 50 3 × 3 × 25 convolutions with stride 1, 2x2 maxpooling, 50 3 × 3 × 50 convolutions, 100 3 × 3 × 50 convolutions, 2x2 maxpooling, 100 3 × 3 × 100 convolutions, global average pooling, 20% dropout, and a single linear output. All layers used SELU activations. This network was applied to the image acquired by each camera independently, and then outputs were summed across views and passed through a sigmoid nonlinearity to predict the probability of a bird carrying a seed for each frame. A hierarchical network combining simultaneous information from all 6 views was then trained end-to-end on manually annotated images.

The outputs of both the bottom camera and the seed carrying network predictions were then input to a user GUI used to annotate all of a bird's cache site interactions in a semi-automated manner. We used a heuristic algorithm, described below, to identify possible interactions involving a cache or retrieval. We then generated flags requiring manual user review whenever our two independent algorithms were in disagreement. The first algorithm detected all times when the bird began or finished carrying a seed in its beak. If a bird gained a seed during a site manipulation, the site manipulation was proposed as a retrieval, and if a bird lost a seed it was carrying during a site manipulation, the action was proposed as a cache. The cumulative number of seeds currently in each site was then computed for the entire session. A second algorithm used bottom camera data, and made a prediction about whether a cache site contained a seed immediately prior to and subsequent to the site interaction. A flag was generated if the second algorithm detected an occupied site which the first algorithm predicted as empty, and vice-versa. A flag was also generated if a retrieval was detected from an empty site. The GUI allowed a manual annotator to browse through all flags, viewing the full sequence of all site manipulations and predicted seed contents at a site within that session, as well as behavioral and bottom camera video for each site manipulation. After manual correction by the annotator, the flag detection algorithm was re-run to ensure consistency of all bottom camera and seed carrying predictions with the updated annotations.

Design of the electrophysiology implant

We designed a light-weight implant for electrophysiological recordings during behavior. The implant was designed for use with a 64-channel silicon probe (H6 ASSY-236, Cambridge NeuroTech), glued to an aluminum drive (nanodrive, Cambridge NeuroTech). The probe was connected to a custom built headstage that used a 64-channel amplifier (RHD2164, Intan Technologies). The headstage communicated digitally with a recording system (C3100 RHD USB interface board, Intan Technologies) over a digital SPI connection (C3216, RHD ultra-thin SPI interface cable, Intan Technologies) connected to a motorized commutator (Assisted

Electrical Rotary Joint 24_PZN12, Doric Lenses). To minimize the forces exerted by the cable, strands of a thin elastic string (1 mm Flat Electric Crystal Stretch String) were tied to the cable to provide a low spring-constant force. The probe and drive were designed to fit within a 3D printed protective housing (Clear Resin, Formlabs), which consisted of two components. The top component housed the headstage, which formed its rear wall, as well as the nanodrive and the probe. The bottom component (base unit) was a small part that attached to the skull. The entire assembly was 1.2 g (0.1 g probe, 0.46 g headstage and connectors, 0.28 g nanodrive, 0.35 g housing).

Surgical approach

Our surgical approach consisted of two steps, detailed below. In the first step, the implant site on the brain was prepared, and base unit of the implant was attached to the skull. In the second step, the top component of the implant was attached.

For the first step, chickadees were anesthetized using 1.5% isoflurane in oxygen. An injection of dexamethasone was made intraperitoneally (2 mg/kg). Fluids (0.9% NaCl, 0.1 mL every 45 min) were administered subcutaneously for the duration of the surgery. Feathers were removed from the top of the head around the surgical site, and the surgical site was cleaned using betadine and 70% ethanol solution. The chickadee was then placed in a stereotaxic apparatus, secured by custom designed ear bars and beak clamp. The bird's head was aligned to stereotaxic axes by adjusting the beak clamp to 30° below horizontal. A silver ground wire (uncoated, 0.005″ diameter) was inserted beneath the skull ~1 mm anterior and 2 mm lateral to lambda, over the right hemisphere. A craniotomy and durotomy were then performed covering a 1 × 1 mm area centered 3 mm anterior to lambda and 0.6 mm lateral to the midline, over the left hippocampus. A 3D printed biocompatible resin insert, consisting of a 0.2 mm depth, 1 × 1 mm square underneath a 0.3 mm depth, 1.5 × 1.5 mm square, was inserted into the craniotomy site and cemented to bone. The insert contained a small central slit (0.4 × 0.1 mm) through which silicon probes could be later inserted. After the insert was cemented (RelyX Unicem, 3M), the space above the craniotomy was filled with a protective layer of Kwik-Cast (World Precision Instruments). The 3D printed base unit (Clear Resin, FormLabs) was then cemented into place, centered above the craniotomy and secured to the skull. A removable 3D printed cap was attached to the base unit to protect the craniotomy site. Buprenorphine (0.05 mg/kg) was injected intraperitoneally and the bird was allowed to recover for 1–2 weeks after this initial surgery.

After birds recovered from the initial surgery, a second procedure followed to implant the top component of the device. Birds were anesthetized and given dexamethasone as above, the removable cap was removed from the base unit, and Kwik-Cast was removed to expose the craniotomy site and the insert. Silicone gel (Dow DOWSIL 3–4680) was added to fully cover the exposed brain, insert, and ~1 mm of space above. The silicon probe and nanodrive assembly were then positioned to allow probes to advance through the insert's slit into underlying brain, and the nanodrive was cemented to the skull. The silicon probe and ground wire were connected to the headstage, and the headstage was inserted into protective housing, which was cemented onto the base unit. Birds were given 1 week to recover from this implantation before continuing behavioral and electrophysiology experiments.

Electrophysiology protocol and spiking data pre-processing

We observed that neural signals degraded rapidly when silicon probes were left in neural tissue between experimental sessions. This degradation included decreases in the numbers of units and amplitudes of spikes, as well as increases in electrode impedance. We therefore developed a semi-acute recording protocol. Approximately 15–30 min before recording on an experimental day, the implanted microdrive was used to lower silicon probes to the desired depth in hippocampus. Recording depth was varied across sessions in the same bird, with data reported in this manuscript pooled across depths up to 1.5 mm below brain surface. Immediately following an experiment, probes were fully retracted such that they rested above the brain, with their tips embedded in the silicone gel covering the brain. Despite making repeated recordings along a similar recording track, we observed only gradual signal degradation over weeks of recording. Probe impedances and background noise also remained low throughout experiments when following this protocol.

Electrophysiology data was bandpass-filtered between 1 Hz and 10 kHz before digitization at 30 kHz with 0.2 μV resolution. Acquisition software simultaneously recorded the digital trigger used to acquire each frame of the behavioral video, for posthoc alignment. At each time point, the median across all channels was subtracted from all signals, and spikes were then extracted by the Kilosort 2.0 algorithm.[84]

For all units extracted by Kilosort, we collected a number of spike metrics used for both quality control and classification of excitatory and inhibitory units. First we obtained the average spike waveform, and from it calculated the spike width, asymmetry, the ratio of the peak and trough of the spike, and the ratio of the peak and trough of the waveform derivative. We additionally calculated the mean rate and a burst-index given by the ratio of the inverse median interspike interval and mean rate. Some of these features have been previously used to distinguish putative excitatory and inhibitory neurons in the avian hippocampus.[48] For quality control, we calculated the spatial extent of each unit along the probe, as well as the cluster contamination rate determined by Kilosort. All units were visualized using a tSNE embedding of these features, and manual clusters were identified for artifacts and neural spikes. A Gaussian mixture model was fit to these manually determined clusters and used to classify all units using the metrics described above. Artifacts had large spatial spread, high contamination rates, and/or unusual waveform shapes compared to neurons. Neurons were subdivided into three groups. Inhibitory neurons had higher and less bursty rates, with narrower and more symmetric spikes relative to excitatory neurons. Some neurons had properties intermediate between clearly excitatory and inhibitory clusters, and were labeled as unclassified neurons.

Spike times were aligned to behavioral videos, and spike counts were binned at 60 Hz. For analysis of single units, we considered only units classified as excitatory or inhibitory neurons, with contamination rates <0.2, and mean firing rates above 0.02 Hz. For population analyses, we included unclassified neurons, and neural units with contamination rates up to 1.

Population firing rate deviation

To quantify deviations in firing rate, we counted, for each neuron, the number of spikes in a sliding 1 s window. We then computed the probability of observing that spike count in a Poisson process whose rate was equal to the neuron's average firing rate across the session. We defined firing rate deviation as the negative log of this probability. This value was low whenever the neuron was firing close to its average firing rate; it was high whenever the neuron was firing either above or below its average rate. To compute the population firing rate deviation, we summed values from all neurons and z-scored the result across the session. To measure population firing rate deviation for a specific event (cache, retrieval, check, or visit), we used the 1 s window centered at the offset of the event.

Single-neuron place and cache tuning

Place maps were obtained by smoothing visit data to each perch with a LOESS quadratic model (MATLAB function *fit* type *loess*, with span 0.4). To quantify the significance of place tuning, we generated 1000 shuffle samples by circularly permuting neural data relative to the sequence of visit locations. For both the real data and the shuffled samples, we computed the standard spatial information index in bits per unit time.[87] A cell was considered to be a place cell if the spatial information for the real data exceeded 95% of the shuffles, computed separately for each neuron.

To quantify the sparsity of cache responses, we calculated the fraction of caches for which a neuron's firing rate was above its firing rate averaged across the entire session. For most excitatory neurons, which had average rates <1 Hz, this threshold was surpassed if any spikes occurred during a cache. Again, we compared this fraction to 1000 shuffled data points. In this case the shuffle distribution was generated by circularly permuting cache times relative to neural spike times. We used the 5^{th} and 95^{th} percentiles of the shuffled distribution to classify neurons as significantly suppressed or enhanced.

Population vector correlation-based analyses

We normalized each unit's firing rate for population analyses by first subtracting its baseline rate, computed as a running 30 min average. After baseline subtraction, we divided firing rate by its standard deviation, which was regularized by adding a small number (0.6 Hz). Most analyses of barcodes and reactivation used a similar analysis framework based on correlating pairs of neural population vectors for two events in the same session. For all analyses, before calculating correlations, the mean across all instances of an action (i.e., across all locations) was subtracted from each instance. For example, the mean across all caching events in a session was subtracted from each caching event. Pairs of events separated by less than 1 min were excluded from the analysis. To obtain standard errors, the analysis was repeated 100 times while resampling with replacement the 54 sessions included in the full dataset. An exponential function with independent parameters for baseline, tau, and amplitude were fit to the data, excluding correlations between events at the same site involving any non-visit action. For analyses involving linear mixed-effects modeling, we used *fitlme* (MATLAB, 2022b) to fit the model and perform t-tests on the significance of each fixed effect.

The robustness of spatial coding is typically assessed using data averaged over long periods of time – e.g., correlating spatial maps from one-half of a behavioral session to another.[48,88] For typical session durations and smoothing parameters, these kinds of analysis in the hippocampus have produced average correlation values of ~0.5. Repeating these analyses for our dataset produced similar values. However, analysis reported in this paper is unusual in that it samples spiking during very brief single events, lasting ~1 s. As expected from the variability of single trial spike counts in brief windows, the resulting correlation values were much smaller (0.024 for the average visit-visit correlation across the dataset). All population vector correlations in the manuscript were multiplied by a constant factor (40.95) such that the value of the exponential curve for visit-visit correlations at the same site was exactly 1.

Place code subtraction

We developed a method to estimate and remove the place code from caching data, in order to isolate the barcode component of activity during caching. For each site in the arena, we first estimated the place activity of each cell, by holding out that site and smoothing data from all perch arrivals at other sites using a LOESS quadratic model (MATLAB function *fit* type *loess*, with span 0.4). For this estimation, we included data from all perch arrivals including both those with and without site interactions. This procedure thus uses data from all other locations in the arena to estimate the smooth spatial component of a neuron's activity, while excluding any contribution from site-specific activity during actions at a particular site. Place activity values across all neurons were combined into a "place vector" defined at each site. The mean value for each neuron across sites was subtracted, similarly to the way cache activity had been mean-subtracted, and place vectors were normalized to unit length. Finally, we computed the projection of cache activity onto this unit vector and subtracted it from the cache activity. This procedure avoids assumptions about how consistent the strength of place coding was across caches, sessions, and birds. "Barcode" activity in this paper refers to activity during a cache after this place subtraction procedure.

1D behavior on a circular track

For 1D behavior, an arena was constructed similarly to the 2D arena described above, but with only 20 perches arranged in a circle of 49.1 cm diameter. Perches were oriented tangentially to the circle. The arena was positioned in a square 60 × 60 cm enclosure. Motorized feeders (3D printed, white resin) were placed in the corners of this enclosure, on the outside of the circular track next to four of the perches. On top of each feeder was a small well filled with water, which was available at all four feeders even when the feeders were closed. Cache sites were placed on the outside of the track next to the other 16 perches, centered at 52.8 cm diameter. This dimension meant that the midpoints between the perches and sites were on a circle of circumference 160 cm—i.e., we considered 8 cm to be the arc distance between two adjacent sites. The cache sites used a previously published,[34] version of the design.

Each bird was typically recorded in 12 sessions on separate days, with at least one day of rest between sessions. One of the feeders was chosen as the "rewarded" feeder for the first three sessions, then a different feeder was chosen for the next three sessions, and so on. For each bird, the four feeders were rewarded in a different random sequence. Each session started with the feeder closed for 10 min and ~3 of the sites baited. The rewarded feeder was then opened for 5 min every 30 min for the duration of the 1.5–2 h session.

One camera (Edmund Optics, EO-2323C) was mounted on the ceiling of the enclosure and used to monitor the position of the bird. Do detect position, we used a neural network[89] trained on the center of the bird's head. A second, identical camera was mounted in the wall of the enclosure. A third camera (Edmund Optics, acA2500-60uc) was mounted under the floor of the arena and used to monitor the contents of the caches. Caches, retrievals, and checks in the 1D arena were detected using a semi-automated annotation procedure.[34]

Calcium imaging

Experiments on the circular track were performed before our lab had developed technologies for silicon probe recordings. For these experiments, we used calcium imaging with head mounted microscopes. Calcium imaging did not allow some of the analyses that we performed in the 2D arena (e.g., analysis of inhibitory cells or the highly temporally precise analyses of neural dynamics). However, it provided comparable numbers of recorded cells per session and could be used for analyzing the spatial code – which was the main purpose of the circular track.

Surgery for calcium imaging consisted of injecting a virus containing GCaMP6f, as well as implanting a GRIN lens and baseplate, using procedures previously described.[50] Anesthesia, initial preparation of the bird, and analgesia were done as for silicon probe experiments described above. Six small holes were drilled through just the top layer of the skull, for the purpose of anchoring the implant. The main craniotomy was then made, centered at 3.25 mm anterior and 0.7 mm lateral to lambda. Before the craniotomy on the inner layer of skull, an antibiotic solution (Baytril 3.8 mg/mL) was applied to the surface of the skull for 5 min, then wicked away. Insect pins were inserted through neighboring pairs of the anchor holes, and both the insect pins and the anchor holes were covered with cement (D69-0047, Pearson Dental). The craniotomy and durotomy were then completed.

Birds were injected with the AAV9-CAG-GCaMP6f-WPRE-SV40 virus (100836-AAV9, Addgene). The total amount of virus injected was 897 nL (65 injections of 13.8 nL each), using a Nanoject II (Drummond Scientific) with a pulled glass pipette tip. Throughout the injection, the surface of the brain was covered in Kwik-Sil (World Precision Instruments). There was a 10 s waiting period between injections, and a 25 min waiting period after the final injection, before withdrawing the pipette and removing the Kwik-Sil.

Before implanting the GRIN lens, the head was angled into a typical chickadee resting head posture (beak bar approximately 10° below the horizontal). A GRIN lens (1 mm diameter, 4 mm length, 1050–004595, Inscopix) was implanted directly over the injection site, any remaining exposed brain was covered with Kwik-Sil, and the lens was anchored in place using cement (D69-0047, Pearson Dental). Next, a baseplate was positioned into a good focal plane with the Inscopix miniscope (focusing slightly below the brain surface, with the miniscope objective approximately 300 μm above the surface of the GRIN lens), and the baseplate was cemented in place. The surface of the cement was covered with black nail polish to prevent light contamination.

Inscopix microscopes have a heavier cable than our silicon probe implants. To support the weight of the cable, birds were therefore fit with a leg-loop harness[90] two weeks after surgery. The harness remained permanently on the bird and consisted of a 3D-printed plastic attachment for the cable (20 × 10 × 6 mm) pressed against the bird's back and two loops of elastic string (39 mm for each leg, Outus Elastic Cord) that were hooked onto the bird's thighs. During behavioral sessions, the microscope was snapped into the magnetic headplate, and the cable at a point ~13 cm from the microscope was attached to the harness.

Analysis of calcium imaging data

For analysis of calcium imaging data, we use procedures previously described.[50] Imaging data were collected at 20 fps. Neuronal traces were extracted from raw fluorescence movies using a constrained non-negative matrix factorization algorithm intended for 1-photon calcium imaging data (CNMF_E[85,91]). We used a multi-scale approach[92,93] to extract stable fluorescent traces from long videos (2 h in our case). Before applying CNMF_E to the raw videos, we applied a motion correction algorithm.[94] The vast majority of data contained no motion above 1 pixel RMS shift.

The multi-scale CNMF_E approach was run in three steps. First, data were averaged in bins of 20 frames, then temporally downsampled by a factor of 20. Cell footprints were found in the downsampled movie using the standard CNMF_E algorithm. These

footprints were then used to extract temporal traces on segments of the non-downsampled data. Finally, the raw traces were deconvolved to detect the time and amplitude of each calcium event. To eliminate some infrequent imaging artifacts, any calcium events with an amplitude greater than 1.5 times larger than the 99th percentile of all calcium events for that cell were eliminated from all analyses. For all firing rate calculations in the paper, events were weighed by their amplitude.

Effects of caching on the place code

To determine the effect of caching on spatial tuning, we used data from the circular track described above. For most analyses, the bird's position was classified as being at one of 20 sites if the radius from the center of the arena was between 19.75 and 30 cm, and the angle was within ±9° from the center of the perch of the site. For the distribution of place fields shown in Figure 4, the circular track was instead divided into 60 segments 6° wide, with every third segment centered on a perch.

For each cache and each cell, we first calculated the spatial tunings of the cell before and after the cache. For pre-cache tuning, we used the time period starting at the last cache or retrieval that previously occurred at the same site; if no such event occurred, the period started at the beginning of the session. The period ended 5 min before the cache. For post-cache tuning, the period started 5 min after the cache and ended at the next cache or retrieval, if such existed, or at the end of the session. Periods of 5 min before and after the cache were excluded because behavior during these periods was typically very different from other parts of the session when the bird moved mostly consistently around the circle. We also excluded periods of ±500 ms around checks during both the pre- and the post-cache periods. For both periods, we determined the number of calcium transients and the behavioral occupancy at each of the 20 sites in the arena. If any site had <1 s occupancy either before or after the cache, the cache was excluded from the analysis. Calcium transient counts and occupancy were each smoothed by a 3-point square window, and firing rates were calculated by dividing smoothed counts by smoothed occupancy values.

We compared pre-cache and post-cache tuning using four metrics. The first metric was the relative difference in peak firing rates, measured as the absolute difference between pre and post values, divided by the average of those values. For this analysis, peak firing rate was defined as the maximum of the 20 values across sites. For the remaining metrics, we only included cells whose peak firing rate was >1 event/s in both the pre and post periods. The second metric was the absolute difference in the positions of the peaks in spatial tuning, measured as the length of the shortest arc around the circular track between these positions. The third metric was the relative difference in the widths of the tuning curves, again measured as the absolute difference divided by the mean. Width was defined at half of the maximum of the tuning curve. The fourth metric was the cross-correlation of the pre and post tuning curves.

To compute statistical significance of each of the four metrics, we generated 100 shuffle samples in which the entire set of times included in the pre and post periods was shifted in time by a random amount, but ensuring that the entire pre and post periods continued to overlap with the session. The 99% confidence intervals for each of the metrics were then computed as 2.8 standard deviations of this shuffle distribution.

Seed tuning

We determined the significance of the modulation of each neuron's activity during checks by the occupancy of the site. For each neuron, we generated single trial responses by calculating firing rate in the window from 100 to 1000 ms from each check onset, and subtracting the baseline rate in the 1000 ms before check onset. These difference were then separately averaged across all checks of empty sites and all checks of sites occupied by a seed. Seed tuning was calculated as the difference between the average occupied and empty responses. To determine significance of this tuning, we generated 1000 shuffle samples by circularly permuting site occupancy assignment (occupied or empty) with respect to neural data during the checks.

Population projections of place code, barcode, and seed code

To obtain the time course of population coding for place, barcode, and seed components, we defined three population vectors. The population vector for seed coding was defined as the difference in check responses for occupied versus empty sites, using the procedure described above, measured across all neurons. The place code vector was defined as that obtained using the leave-one-out procedure described above for place code subtraction. The barcode vector was defined as the average barcode activity (i.e., activity during caches after place code subtraction) across all caches at a site. All projections were cross validated by recomputing vectors for each event while holding out the data to be projected. Standard errors were computed by 1000 bootstrap samples, drawing with replacement from the 54 session-averaged projection time courses.

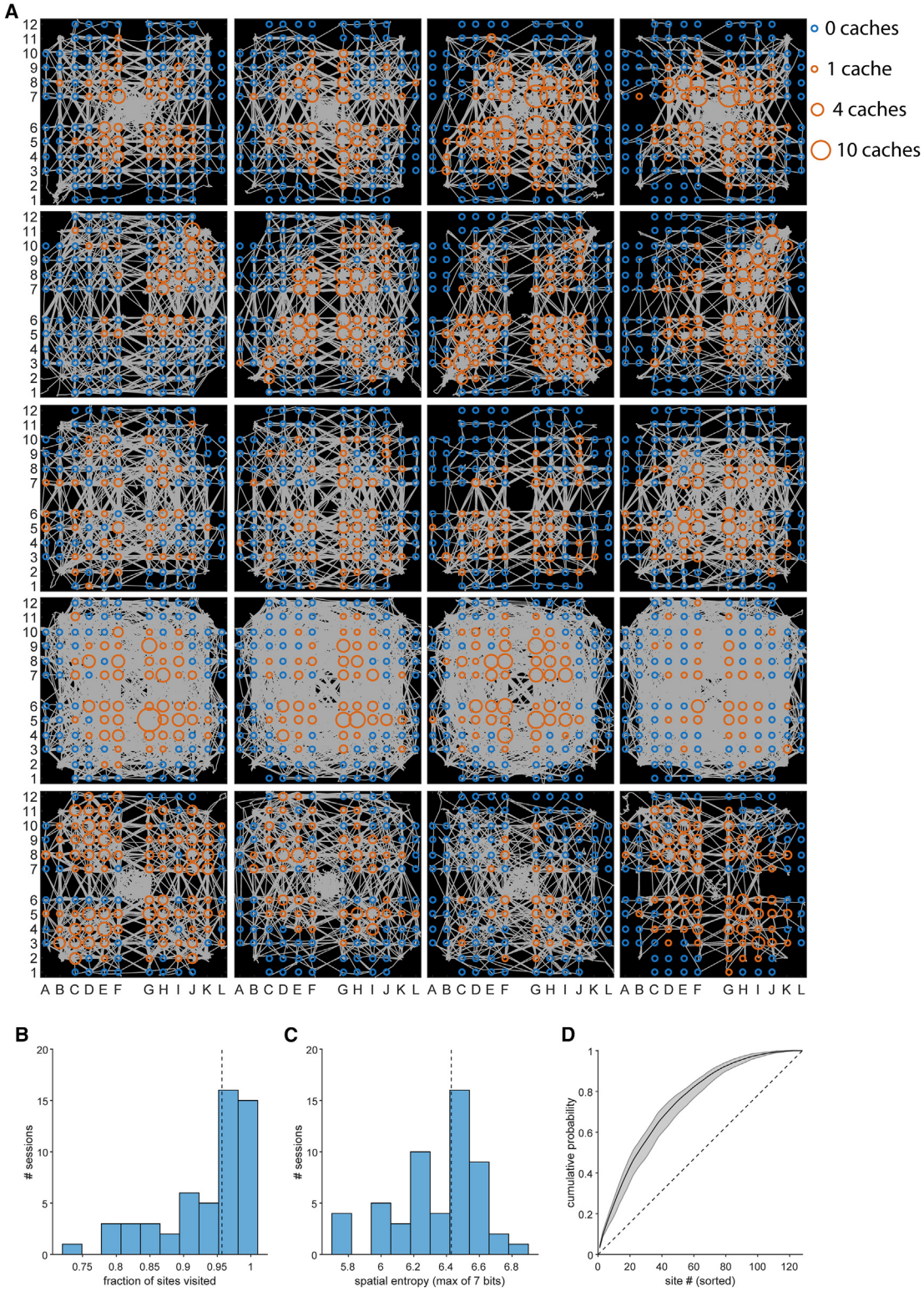
Histology

After completion of the experiments, animals were administered ketamine and xylazine (10 mg/kg and 4 mg/kg respectively), then transcardially perfused with 1X PBS followed by 4% paraformaldehyde in PBS. The brains were extracted and stored in 4% paraformaldehyde in PBS for 2 days. They were then sectioned coronally into 100 μm-thick slices, stained with fluorescent DAPI (300 nM in 1X PBS, D1306, Invitrogen) and mounted in Vectashield mounting medium (H-1400-10, Vector Laboratories). Slices were imaged with an epifluorescence microscope to confirm recording locations.

QUANTIFICATION AND STATISTICAL ANALYSIS

Unless a conventional statistical test is specifically noted, statistical quantification of error was performed using a bootstrap. Specifically, we selected 54 sessions randomly with replacement from the full set of 54 sessions. Analyses were then performed on this resampled data, and the process was repeated 100 times. The standard deviation across bootstrap samples was reported as the standard error of the mean in all figure panels. Unless otherwise noted, statistical quantification of significance was performed using a shuffle-based procedure described in the appropriate method details subsection. No experimental subjects were excluded, and data from all sessions from all subjects were included unless the bird made less than 30 total caches in a session, we identified less than 50 units in electrophysiological data, or data were otherwise corrupted.

Supplemental figures



(legend on next page)

Figure S1. Birds used sites across the entire behavioral arena, related to Figure 1

(A) Behavioral trajectory plots for 20 example sessions. The bird's 2D body position is plotted in gray, and each cache site is overlaid with color and size indicating cache site usage. Each row of plots is sessions from one of the five birds in this study. Four example sessions are shown for each bird, sorted from highest (left) to lowest (right) by the entropy of the distribution of perch arrivals.

(B) Fraction of sites visited by a bird within each session, n = 54 sessions. Dashed line is median.

(C) Entropy of the within-session distribution of perch arrivals across all 128 sites.

(D) Cumulative probability of the within-session distribution of perch arrivals after sorting sites for each session from most to least common. Solid line and shaded area are mean and 25^{th}–75^{th} percentile intervals across all 54 sessions. Birds were not encouraged to use sites evenly and exhibited diverse and variable spatial biases but nevertheless visited and cached at most sites in the arena.

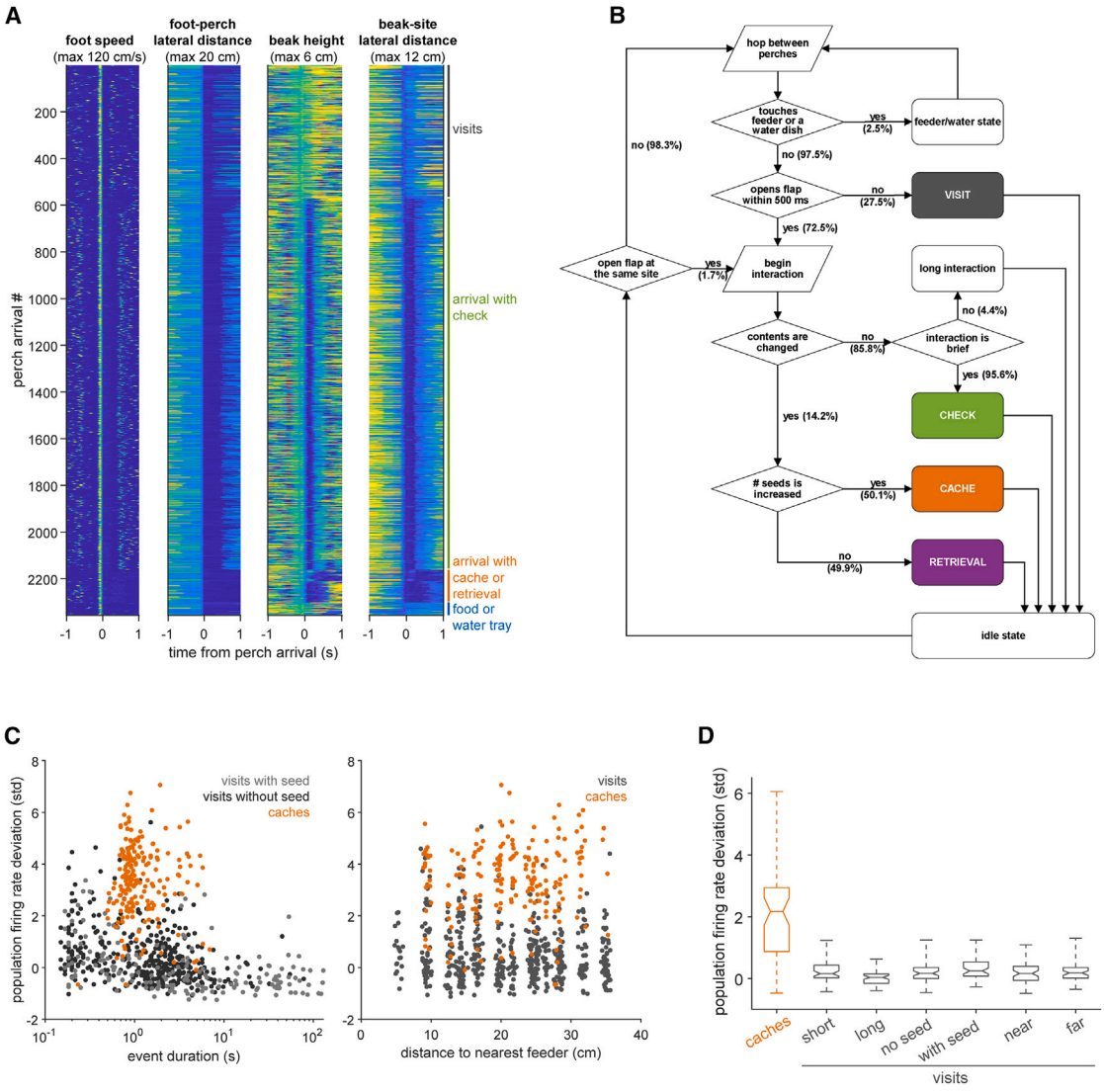


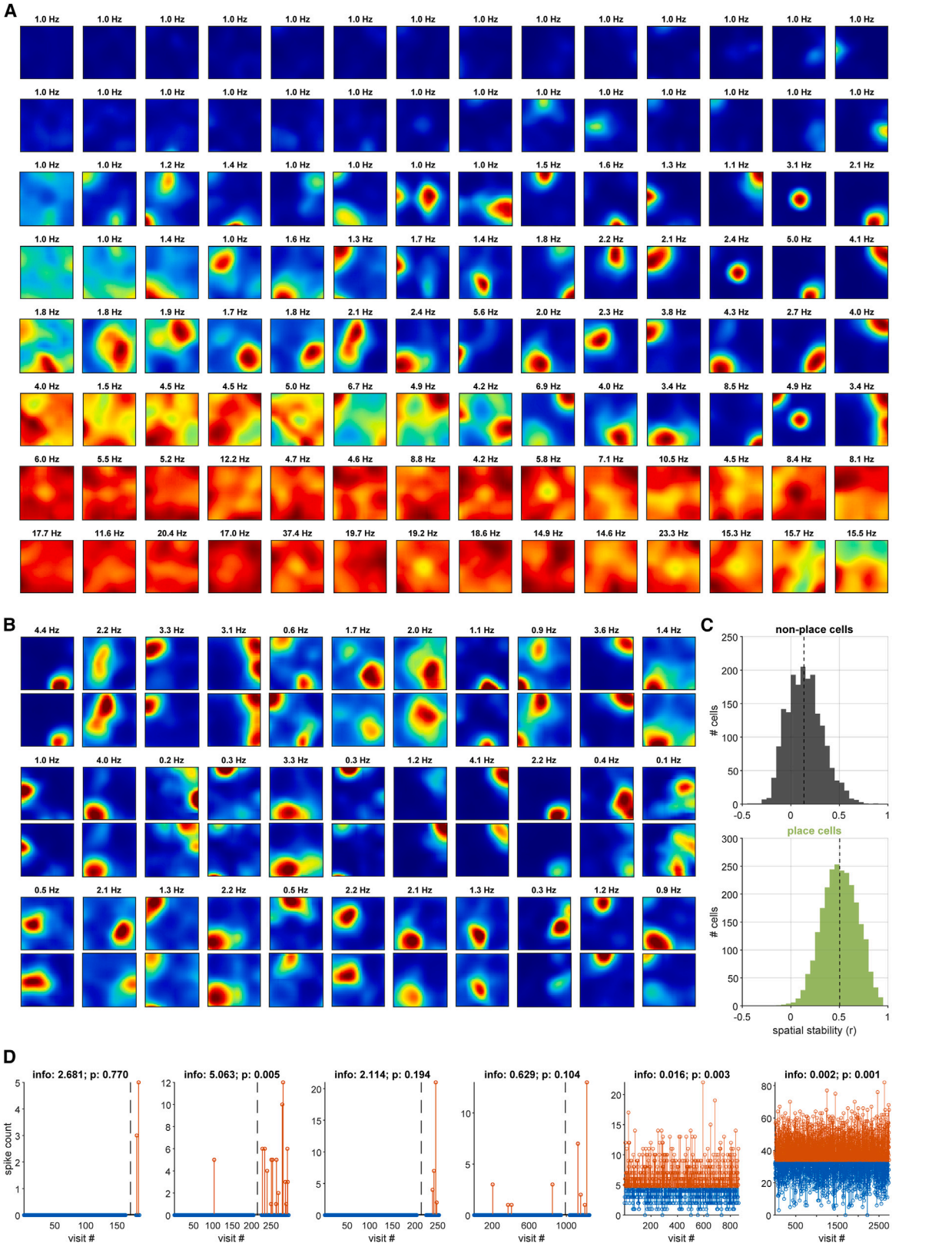
Figure S2. Caches elicited distinct hippocampal activity, related to Figure 1

(A) Behavioral tracking variables used in action identification for one example session. For each arrival at a new perch, heatmaps show from left to right the speed of the centroid between the two feet, the lateral distance between the foot centroid and the centroid of the new site's perch, the height of the beak tip above the arena surface, and the lateral distance of the beak tip from the centroid of the new site's cache site. The color of each heatmap ranges from 0 to the maximum indicated in each plot's title. Arrivals are grouped by the identified action, indicated on right.

(B) Flowchart schematizing the action identification algorithm. The algorithm begins with identification of a hop between perches and proceeds through a series of binary decisions, with the frequency of both outcomes across the entire dataset indicated. Action times are aligned to the hop or to the site interaction if identified. See STAR Methods for full definition of algorithm and temporal windows. The vast majority of events were classified as one of the four actions (visit, check, cache, and retrieval) analyzed throughout the manuscript.

(C) Population firing rate deviation for all caches and visits in the example session from Figure 1D. Left: each event is plotted against event duration. Visit events are colored by whether the bird was carrying a seed in its beak (light) or not (dark). Deviation was measured in the 1 s window centered at event offset or at the midpoint of the visit for visits exceeding the median cache duration. Right: population firing rate deviation as a function of distance from the nearest feeder. The increased population firing rate deviation for caches compared to visits is not accounted for by variables such as event duration, seed carrying, or arena position.

(D) Population firing rate deviation for caches and visits segregated by control variables. Visits within each session were split in two in a series of three comparisons. First, visit durations were compared to the median total latency from perch arrival to cache offset in that session. For visits with shorter duration ("short"), deviation was measured at visit offset. For visits with greater duration ("long"), deviation was measured at the latency matching cache offset. Second, visits were split by whether the bird was carrying a seed in its beak when arriving at a site ("with seed") or not ("no seed"). Third, visits were split by whether they occurred at sites closer ("near") or farther ("far") from the nearest feeder than the within-session median across visits. Box and whisker plots show the distribution of within-session medians across all 54 sessions, computed as in Figure 1E. Whiskers range from minimum to maximum, boxes are 25^{th}–75^{th} percentile, line is median, notches indicate significant difference in the median at 5% level if notched intervals do not overlap. Caches exhibited population firing rate deviations much greater than visits in all cases.



(legend on next page)

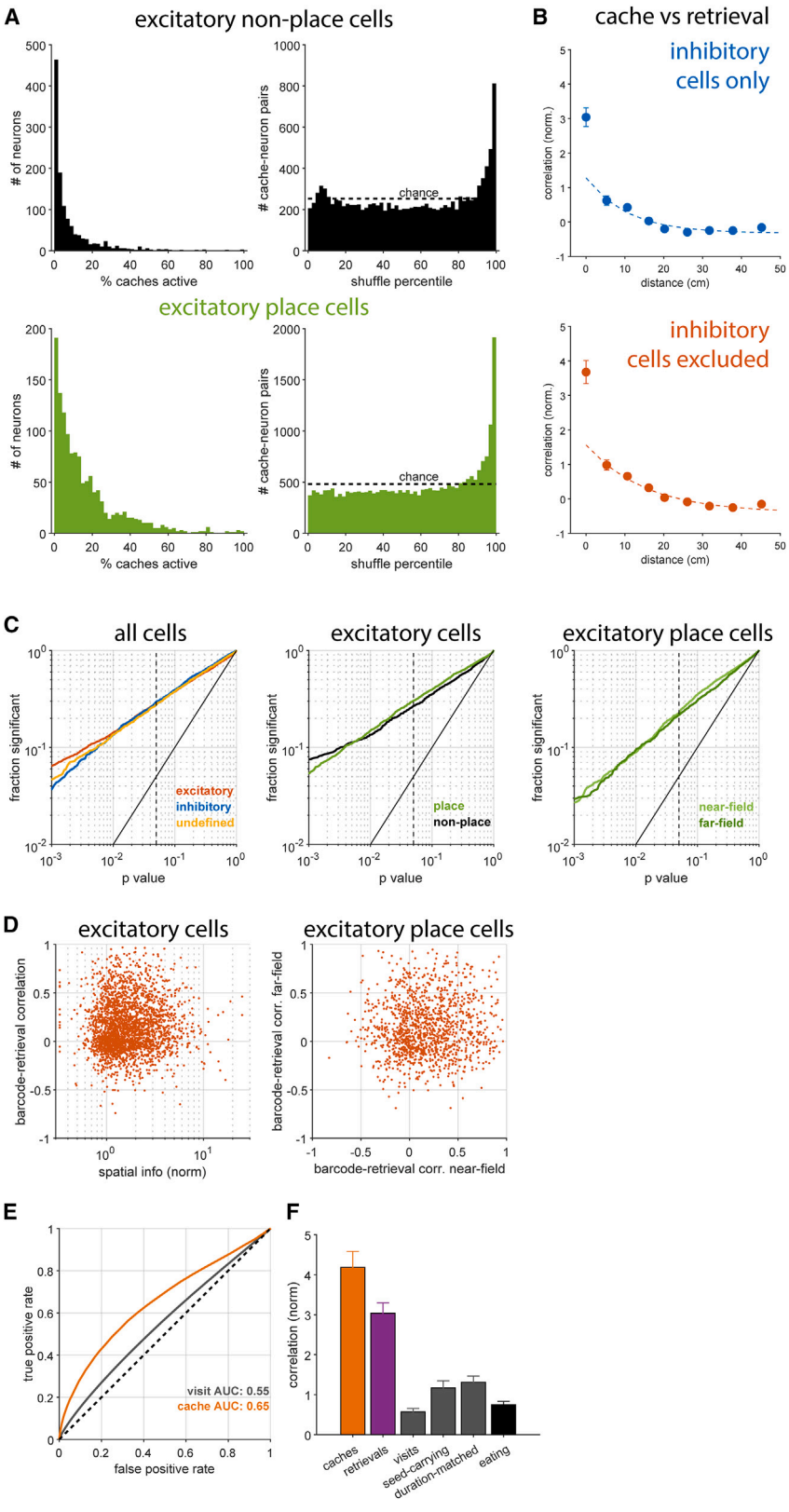
Figure S3. Individual neurons showed typical place tuning, related to Figure 2

(A) Place maps for 112/116 single units recorded in an example session; for figure layout reasons, four silent neurons are not shown. Neurons were sorted into eight rows by the average firing rate and then within each row by low-to-high spatial information from left to right. Each plot's color ranges from 0 to the place map maximum shown in title or to 1 Hz for neurons with map peaks below 1 Hz. Neurons with high firing rates were often interneurons.

(B) Place maps for 33/43 excitatory place cells, randomly selected from the same example session. Maps were computed on separate halves of the data after segmentation into non-overlapping 5 min periods, as in previous studies.[48] Unlike in the rest of the manuscript, where place maps are computed for visits at each site and interpolated for display purposes, place maps in (A) and (B) are computed following convention for analyzing open-field data[48] to simplify comparison.

(C) Stability of spatial tuning for all single units; dashed line indicates median. Maps were computed on separate halves of the data after segmentation into non-overlapping 5 m periods.[48] Place maps for each half were computed for visits at each site, and the Pearson correlation was computed between the two maps. Histograms are shown separately for neurons that did not (top) or did (bottom) pass the shuffle-based place cell criteria used throughout this manuscript. Note that spatial stability was not used to define whether cells were place cells. Spatial stability in our data was similar to values reported in previous studies.[48]

(D) Spike counts on individual visits for the six example neurons in Figure 2A. Plots follow the same convention as Figure 2A, where trials with above- or below-average rates are colored red or blue, respectively. The spatial information in bits/spike and the significance of spatial tuning compared to shuffle is indicated in plot titles. For excitatory neurons (first four from left), visits were divided into out-of-field and in-field visits, shown to the left and right of the dashed line. "In-field" was defined as sites where the place map was more than one-fourth of the maximum, and "out-of-field" was defined as sites where the place map was equal to or below the map median; the small number of remaining visits are not shown. Excitatory place cells (e.g., second neuron) showed large variability in spike count between repeated visits of in-field sites. Inhibitory neurons (last two) did not show consistent increases or decreases in rate during visits, unlike changes observed during caching (compare to Figure 2A).



(legend on next page)

Figure S4. Place coding and barcoding are randomly mixed in hippocampal activity, related to Figure 3

(A) Analysis activity during caching as in Figures 2B and 2C but separately for place and non-place cells. Left: fraction of caches on which a neuron responded (i.e., exceeded mean firing rate). Right: comparison of cache responses to shuffle distribution. Both place and non-place cells were sparsely active during caches, although place cells were less sparse, likely because they also exhibited place activity during caches within their place fields. Both place and non-place cells had large bursts of activity during caches.

(B) Population vector correlation of neural activity between cache and retrieval pairs as a function of distance. Analysis as in Figure 4G but using only inhibitory neurons (top) or without inhibitory neurons (bottom). Results were similar, demonstrating a combination of smooth spatial tuning and reactivation of a site-specific barcode.

(C) Fraction of neurons with a significant barcode-retrieval correlation for a range of p values. Single-neuron barcode-retrieval correlation was calculated by computing barcode activity as described in the main text and assembling a vector for each neuron of its barcode activity across all sites (averaging across multiple caches at a site when applicable). A similar vector was assembled for retrievals, and vectors were then correlated across all sites with at least one cache and retrieval. Significance was determined by comparing correlation to values obtained after randomly permuting the barcode and retrieval vectors. Dashed vertical line is $p = 0.05$. The analysis is repeated for all neurons grouped by cell type (left) and all excitatory neurons grouped by place tuning significance (middle). The analysis was also repeated for all excitatory place cells (right) after evenly dividing the arena into sites near or far from the neuron's place field maximum. Barcode tuning was similar in all cases.

(D) Left: spatial information of a neuron's place map plotted against single-neuron barcode-retrieval correlation. Spatial information was normalized by dividing the raw value by the mean of the shuffles. The plotted relationship was very weak ($r = 0.058$, $p = 0.004$, Spearman's correlation). Right: barcode-retrieval correlations after dividing the arena into halves either closer to or farther from the maximum of each place cell's firing field. Place cells participated in barcodes near and far from their place fields, although there was a small but significant difference in mean correlation (near, 0.17; far, 0.14; $p < 0.01$, t test). Barcode activity was thus mostly unrelated to the strength and location of place tuning.

(E) Population decoder performance. The decoder converted a population vector correlation between two events to a binary prediction of whether the events occurred at the same or different sites. A receiver operating characteristic (ROC) plot of performance across thresholds is shown with the area under the curve (AUC) for visit-visit and cache-cache pairs. During caching, there was an elevation in site-specific activity compared to visits.

(F) Population vector correlation between a barcode and activity during other events at the same site. For visits, this was also computed for the subset where a bird was carrying a seed in its beak ("seed-carrying"). This was also computed for visits with duration at least as long as retrievals, using the latency and duration of the median retrieval on that session ("duration-matched"). "Eating" events used a window of equal duration to visits, centered in the middle of an eating bout. Barcode reactivation was much greater for events involving site interactions (caches and retrievals) than those without interactions (visits and eating). Error bars: SEM computed by bootstrapping data from all 54 sessions.

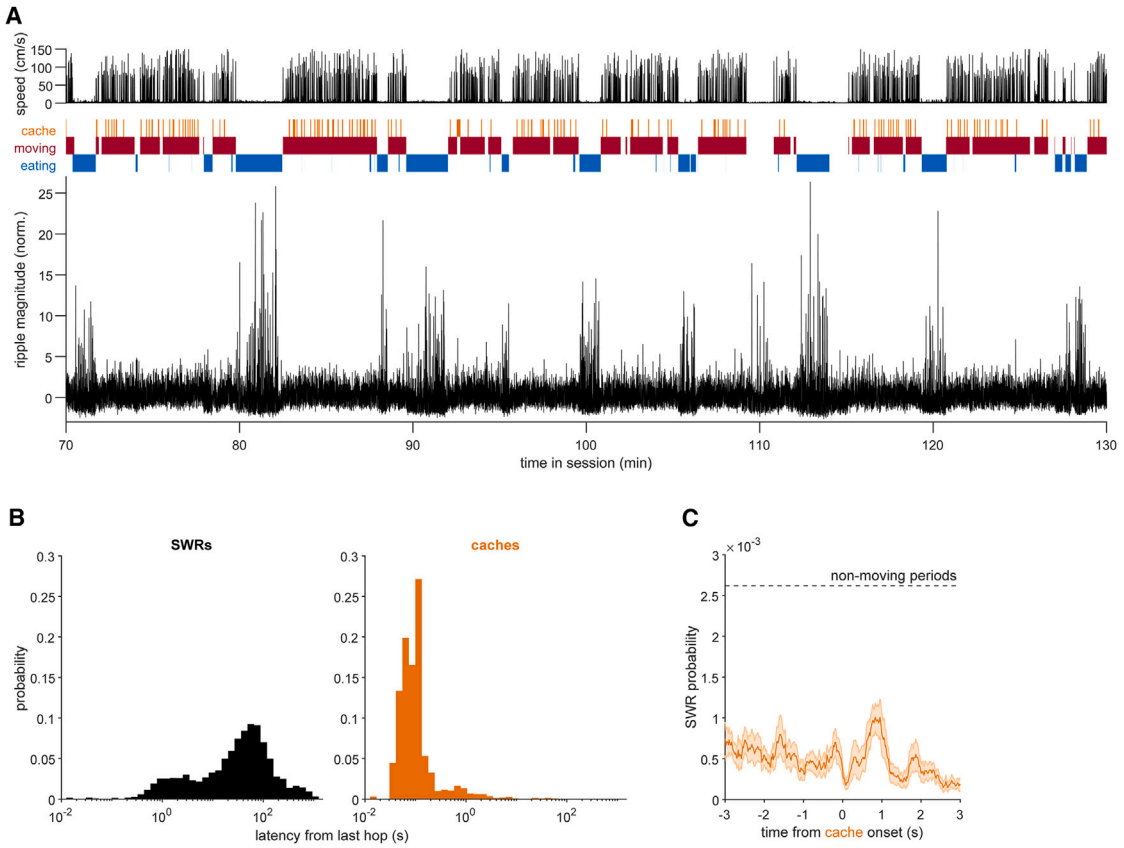
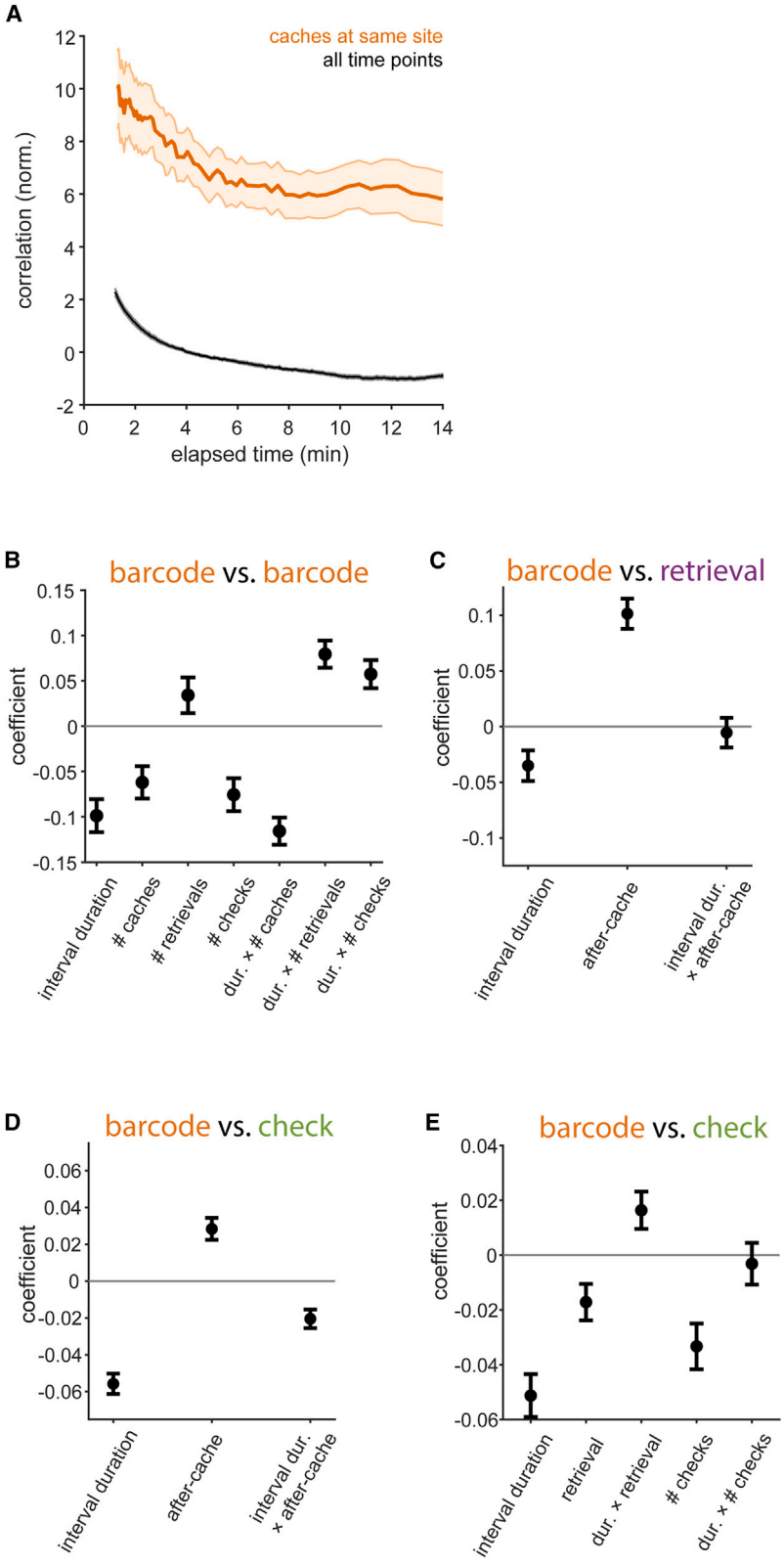


Figure S5. Sharp-wave ripples did not occur during caching, related to Figure 2

(A) Ripple-band magnitude (100–200 Hz, as in Payne et al.[48]) plotted for 1 h of an example session. Linear speed of the centroid between the bird's feet plotted above, along with binary indicators of whether the bird was caching, eating, or in a moving state (the latter defined as in Payne et al.[48]). As in rodent studies, large transient bursts in ripple magnitude (SWR, above ~5 SD) occurred when the bird was not moving, often during eating bouts. Similar events were not observed during caching.

(B) Latency between onset of an SWR (left) or a cache (right) and the bird's last hop to a new perch. Caches typically occurred <0.2 s after arrival, whereas SWRs occurred >1 s after arrival. Thus, caches and SWRs occurred at characteristically different times, during active behavior and during immobile periods, respectively. Because local field potentials in some birds and sessions were contaminated by movement or other artifacts, SWRs for this analysis were detected by summing spike counts across all units in 1/60 s bins and identifying threshold crossings above 5 standard deviations. This count was highly correlated ($r \sim 0.8$) with ripple-band magnitude in sessions with clean local field potential signals, consistent with previous literature. Data from 28/54 sessions that had at least 92 recorded units.

(C) Probability of an SWR as in (B), aligned to cache onset times. Dashed line is the rate of SWRs measured during immobile periods. SWRs did not reliably occur during caching, and SWRs were far more likely to occur during immobile periods than during caching. Line and shaded area: mean and SEM, calculated by bootstrap resampling 28/54 sessions with at least 92 units.



(legend on next page)

Figure S6. Barcodes changed with experience at a cache site, related to Figure 5

(A) Black curve: autocorrelation of population vectors calculated on non-overlapping 1.25 s windows. Orange curve is a time-cropped version of Figure 5B. Neural activity was similarly correlated on a timescale of <5 min, regardless of what the bird was doing. This decay is therefore not a feature of barcodes.

(B) Coefficients of a linear mixed-effects model of the correlation between two cache barcodes at the same site. The model contains random effects for each session (not shown) and fixed effects for the duration of time between caches, the number of intervening caches/retrievals/checks, and nonlinear interactions between duration and each intervening event count. Coefficients are without units since variables were *Z* scored before model fitting. All coefficients were significantly different from 0 ($p < 0.001$), except the linear term for intervening retrievals ($p = 0.082$). Model coefficients were consistent with effects shown in Figures 5A and 5B. Specifically, barcode correlations were reduced by both the number of intervening caches and the time between caches. The strongest coefficient was a negative interaction between duration and intervening caches, meaning that decorrelation between barcodes was particularly strong when caches were separated by both a long interval and multiple intervening caches.

(C) As in (B) but for barcodes and retrievals at the same site, with fixed effects for the duration between events, whether the retrieval was after or before the cache, and a nonlinear interaction between the two. Barcode-retrieval correlations were greater for retrievals after a cache than before ($p < 0.001$) and decreased for longer intervals ($p = 0.01$). The interaction term was negligible ($p = 0.69$), implying that the post-cache increase in correlation was temporally stable, consistent with results in Figures 5C and 5D.

(D) As in (C) but for barcode-check pairs. All coefficients were significantly different from 0 ($p < 0.001$), consistent with results in Figures 5E and 5F.

(E) As in (D) but only for pairs where the cache preceded the check with no intervening caches and with fixed effects for duration, whether an intervening retrieval had occurred, the number of intervening checks, and nonlinear interactions between duration and the other two variables. The negative coefficient for retrieval ($p < 0.01$) and its positive interaction with duration ($p = 0.016$) implies that barcode-check correlations were lower after the cache was retrieved, particularly if the duration between cache and check was brief, consistent with results in Figure 5F. We additionally observed effects of duration and intervening checks ($p < 0.001$) with an insignificant interaction ($p = 0.68$).

Error bars in all panels: SEM.

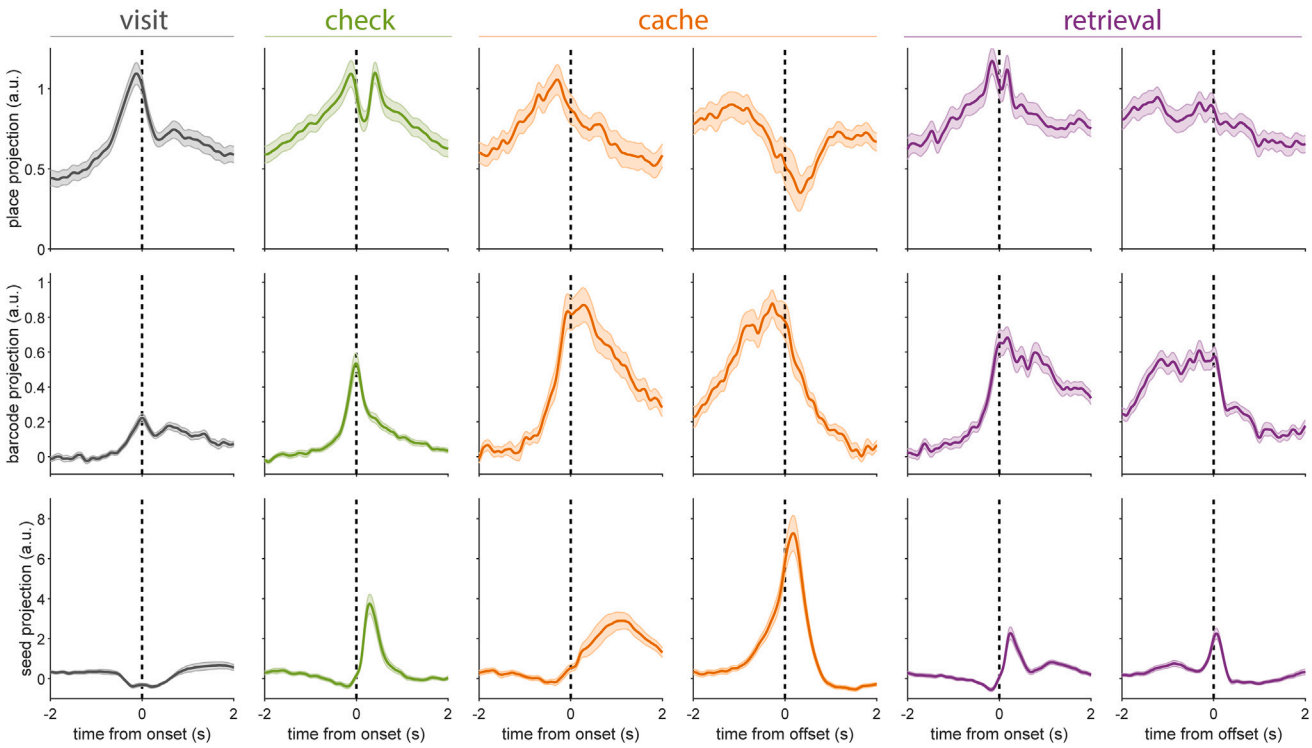


Figure S7. Place, barcode, and seed tuning were coordinated with behavior, related to Figure 7

Projections of neural activity onto dimensions of place, barcode, and seed tuning. Projections are plotted for visits, checks, caches, and retrievals aligned to onset and for caches and retrievals aligned to offset. Projection values were scaled by a constant across all 18 plots such that the place projection for visits at time 0 was equal to 1. For seed projection plots, only data for occupied visits and checks are shown (see Figure 7 for empty visits and checks). The temporal sequence of place, barcode, and seed tuning during checks (of occupied sites) resembled a time-compressed version of that seen during caches, reflecting their briefer duration. Shaded region is SEM with bootstrap resampling, n = 54 sessions.